

1 **Dynamic Infrared Gas Analysis from Longleaf Pine Fuelbeds Burned in a Wind**
2 **Tunnel: Observation of Phenol in Pyrolysis and Combustion Phases**

3 Catherine A. Banach,¹ Olivia N. Williams,¹ Ashley M. Bradley,¹ Russell G. Tonkyn,¹
4 Joey Chong,² David R. Weise,² Tanya L. Myers,¹ Timothy J. Johnson^{1*}
5 ¹Pacific Northwest National Laboratory, Richland, WA USA
6 ²USDA Forest Service, Pacific Southwest Research Station, Riverside, CA, USA
7 *Contact: Timothy J. Johnson, timothy.johnson@pnnl.gov

8
9 **0. Abstract**

10 Pyrolysis is the first step in a series of chemical and physical processes that produce flammable
11 organic gases from wildland fuels that can result in a wildland fire. We report results using a new
12 time-resolved Fourier transform infrared method that correlates the measured FTIR spectrum to
13 an infrared thermal image sequence enabling identification and quantification of gases within
14 different phases of the fire process. The flame from burning fuel beds composed of pine needles
15 (*Pinus palustris*) and mixtures of sparkleberry, fetterbush and inkberry plants was the natural heat
16 source for pyrolysis. Extractive gas samples were analyzed and identified in both static and
17 dynamic modes synchronized to thermal infrared imaging: A total of 29 gases were identified
18 including small alkanes, alkenes, aldehydes, nitrogen compounds and aromatics, most previously
19 measured by FTIR in wildland fires. This study presents one of the first identifications of phenol
20 associated with both pre-combustion and combustion phases, using ca. 1 Hz temporal resolution.
21 Preliminary results indicate ~2.5x greater phenol emission from sparkleberry and inkberry
22 compared to fetterbush, with differing temporal profiles.

23 **Keywords:** Fourier transform infrared, time-resolved, biomass burning, pyrolysis, phenol,
24 benzene, naphthalene, *Pinus palustris*, *Lyonia lucida*, *Ilex glabra*, *Vaccinium arboreum*

25 **1. Introduction**

26 Wildland fire is an important component of many ecosystems and has been used by humans for
27 several thousand years (Crutzen and Goldammer, 1993; Pyne, 1997; Scott et al., 2014). Many
28 North American ecosystems have evolved as a result of persistent fire (Barbour and Billings,

29 2000). The importance of fire in pine forests worldwide including the southern U.S. is well-known
30 (Agee, 2000; Christensen, 2000). In the U.S., prescribed burning is used on approximately 8
31 million ha annually to accomplish a variety of forestry and agricultural objectives (Melvin, 2015);
32 the impact of smoke from these fires has been studied for over 50 years (Chi et al., 1979; Biswell,
33 1989; Ward and Hardy, 1991; Hardy et al., 2001;). In the southern U.S., forest management
34 objectives include hazardous fuel reduction, site preparation, improved wildlife habitat, insect and
35 disease control, enhanced appearance and perpetuation of fire dependent species and natural
36 communities (Carter and Foster, 2004; Waldrop and Goodrick, 2012). The U.S. Department of
37 Defense (DoD) uses prescribed burning on approximately 243,000 ha annually for many of these
38 objectives as well as maintenance of critical training areas (Cohen et al., 2014). Many land
39 managers rely on fire behavior models to calculate fire movement on the landscape, energy release,
40 smoke plume development, dispersion and content (Bytnerowicz et al., 2009, Paton-Walsh et al.
41 2014). However, few fire behavior models account for the plethora of chemical reactions involved
42 in the fire. The heat transfer processes that take place in the fire environment are also only coarsely
43 described. In order to improve the use of prescribed burning to accomplish refined objectives,
44 more detailed description and modeling of the physical and chemical processes in fire are needed
45 (Cohen et al., 2014).

46 The chemical phases of wildland fire, described as preheating, flaming, smoldering and glowing
47 (Ward, 2001) are understood in a chemical sense, but only to varying degrees: While the chemical
48 effluents of flaming and smoldering phases have been characterized for many ecosystems and fuel
49 types at different scales (Ward and Radke, 1993), the physics and chemistry of the preheating
50 (pyrolysis) phase, have fewer studies beyond the bench scale (e.g. Depew et al., 1972;
51 Dimitrakopoulos, 2001; Susott, 1982; Tihay, 2010). To improve fire application models and to
52 accomplish the desired fire effects and limit potential fugitive emissions, improved understanding
53 is thus needed for many fundamental processes, particularly for pyrolysis and ignition in
54 heterogeneous fuel beds of live and dead fuels that reflect the diversity of vegetation found
55 worldwide. (Guérette et al. 2018).

56 Prior to oxidative combustion, biomass thermally decomposes in a heated environment. To study
57 this decomposition, thermogravimetric analysis has been applied to a small set of plant species
58 deemed to represent major wildland fuel types (e.g. Burgan and Susott, 1991; Susott, 1982). Others

59 have determined caloric content of southern fuels which is related to the composition of pyrolysis
60 products (Hough, 1969; Behm et al., 2004). However, most such prior work used dried, ground
61 fuel samples in either an inert or oxidizing environment subject to uniform heating and heat
62 transfer, (Kibet et al. 2012) thereby eliminating the effects of moisture and heat transfer which are
63 key fire behavior variables. While pyrolysis and combustion of wildland fuels is known to be a
64 complex process (Zhou and Mahalingam, 2001), they are often modeled using simple
65 approximations in the relevant computer codes using the dominant gases of H₂, CO, CO₂ and CH₄.
66 Heat transfer in a wildland setting is less efficient than in thermogravimetric analysis: The amount
67 and composition of pyrolyzed species produced depend strongly on heating rate and temperature
68 and typically consists of oxidized small-molecule gases such as CO, CO₂, or H₂O, as well as non-
69 oxidized or partially oxidized species such as H₂, CH₄, C_xH_y, C_xH_yO_z as well as tars. The products
70 of primary pyrolysis may react in the gas phase at elevated temperatures (i.e., secondary pyrolysis),
71 which may affect the amount of tar remaining.

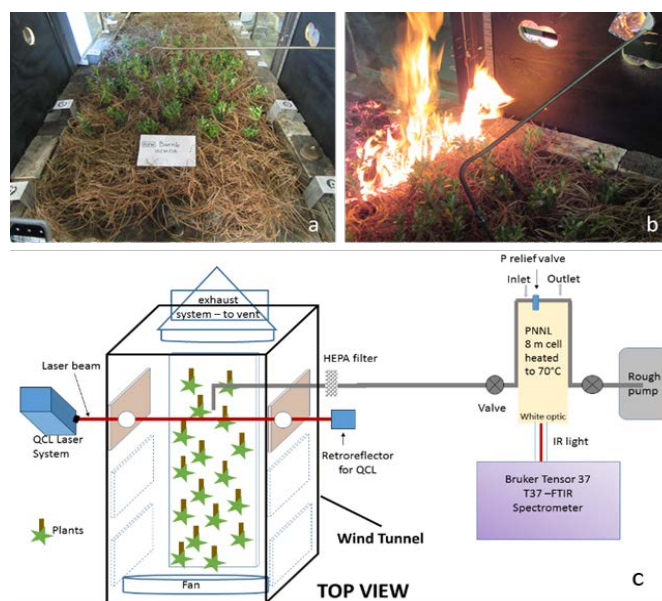
72 This work is part of a larger project to measure and model pyrolysis gases from common wildland
73 fuels found on DoD installations in the southern United States (Weise et al. 2018). The project
74 includes bench-level, laboratory-scale and field plot burns; integrating the results of the field and
75 laboratory measurements with the modeling results to identify potential improvements that can
76 enhance understanding of pyrolysis and ignition in wildland fuels. During the course of the project
77 Fourier transform infrared (FTIR) methods have been used on several occasions to non-intrusively
78 measure the composition and concentration of the pyrolysis gases including the gases liberated by:
79 i) heating single leaf samples from several common southern fuels using different heating modes
80 in a pyrolyzer and in a simple flat-flame burner system, (Amini et al., 2019; Safdari et al., 2020)
81 ii) heating shrubs in prescribed burns at Ft. Jackson, South Carolina, (Scharko et al., 2019a, b) and
82 iii) heating nursery plants with flames from longleaf pine needle fuel beds inside a wind tunnel
83 (Aminfar et al., 2019). In order to achieve the goal that the results be applicable to prescribed
84 burns, a key focus has been linking the bench scale, wind tunnel and field data to the models using
85 realistic values and identities for the pyrolysis gases. Chemical analysis of the foliage and results
86 of the bench scale tests so far suggest that describing wood pyrolysis may not be suitable for foliage
87 fuels (live and dead) (Jolly et al., 2012; Jolly et al., 2016; Matt et al., 2020). To date, pyrolysis and
88 ignition of wildland fuels have typically been based on results for only cellulose or wood (e.g.
89 Varhegyi et al., 1994; Di Blasi, 2008). In this paper a small wind tunnel was used to bridge the

90 bench-scale studies to the field-scale pyrolysis measurements using a subset of the plant species
91 from the bench-scale tests. The wind tunnel measurements were set to emulate the larger scale
92 FTIR experiments using canister samples in 0.1 ha prescribed burns at Ft. Jackson in May 2018.
93 The specific goal is to provide better temporal / flame phase resolution than provided by larger
94 field studies such as the Ft. Jackson burns or from large chamber facilities such as the Fire Sciences
95 Laboratory (FSL) in Montana (Yokelson et al., 1996, Burling et al., 2010); the FSL has long path
96 optical cell coupled to an FTIR as well as many other powerful analytical methods such as proton-
97 transfer mass spectrometry (Christian et al., 2004; Warneke et al., 2011; Yokelson et al., 2013)
98 and has made first detections for dozens of chemical species and pioneered the science of biomass
99 burning in many ways. But because the sampling platform is 4 m above the floor, there is mixing
100 of gases from different phases such as volatilization and pyrolysis. The combustion and smoldering
101 phases are typically easier to differentiate, primarily via the intrinsic diagnostic of the modified
102 combustion efficiency (Ward and Hao, 1991), a measure that is not independent of the composition
103 of smoke (Weise et al 2020). Similar ambiguities as to the nature of the phase of the fire also
104 applies to extractive methods whereby a sampling device attempts to capture pre-combustion
105 phase gases. Such sampling systems, typically connected to a field canister are effective but are
106 subject to vagaries of sniffer gas inlet placement, i.e. proximity to the pyrolyzing plant. (Scharko
107 et al. 2019a,b). Here we describe use of an FTIR with a probe to temporally isolate, identify and
108 quantify some of the early-stage/pyrolysis gases from burns at a mid-scale laboratory facility.
109 Experiments were conducted at the Riverside Fire Lab (RFL) in a wind tunnel using fuel beds
110 composed of longleaf pine needles and the live plants fetterbush, inkberry, sparkleberry and
111 blueberry. Multiple methods were used such as quantum-cascade lasers (Phillips et al., 2020), gas
112 chromatography-mass spectrometry as well as FTIR with the overall objectives of: i) using careful
113 chemometric extraction from the acquired data to see what pyrolysis species can be identified by
114 the techniques; ii) using the various methods to determine the degree of oxidation or combustion,
115 i.e. pyrolysis characterization; iii) making first attempts to quantify the rates of evolution of
116 pyrolysis products for certain plant species; and ideally; iv) determining if differences exist
117 between the pyrolysis emissions / temporal profiles for different plant species. We take advantage
118 of the high resolution and time-resolved capabilities offered by IR spectroscopy and couple these
119 to the flame/solid fuel temperature diagnostics of an IR camera to analyze the emissions from a
120 series of RFL burns.

121 2. Experimental

122 2.1 Wind Tunnel and Experimental Configuration

123 As part of the project a total of 88 laboratory scale burns were conducted at the USDA Forest
124 Service Pacific Southwest Research Station in Riverside, California; this paper reports on the 21
125 burns from November 2018. The Riverside laboratory includes a wind tunnel ca. 3 m long and 1
126 m wide which was set up to simulate a forest floor of litter and live plants. Fuel beds composed of
127 1 kg of dry longleaf pine needles and various combinations of inkberry (*Ilex glabra* (L.) A. Gray),
128 fetterbush (*Lyonia lucida* (Lam.) K. Koch), sparkleberry (*Vaccinium arboreum* L.) and blueberry
129 (*V. darrowii* Camp) were burned under either “no wind” or 1 m s^{-1} wind conditions. Fuel moisture
130 content and mass loading, ambient temperature and relative humidity in the tunnel were varied
131 between experiments; fuel beds were ignited with a line fire which propagated the length of the
132 fuel bed as seen in Fig. 1b. Multiple techniques were used to study the fire characteristics as well
133 as the gas effluents: thermocouples, Schmidt-Boelter flux sensor, nadir thermal IR camera and
134 background-oriented Schlieren photography (Aminfar et al 2019) to estimate heat transfer / air
135 flow around the plants, canister samples analyzed by GC/FID, quantum cascade (QC) infrared
136 laser spectroscopy, (Phillips et al., 2020) as well as broadband Fourier transform infrared (FTIR)
137 spectroscopy. A schematic overview of the experimental setup is seen in Figure 1c.



138

139 **Figure 1.** a) Overhead view of wind tunnel down its length with longleaf pine needles and interspersed
140 inkberry plants; b) flame front progressing down the wind tunnel with FTIR extraction tube visible; c)
141 cartoon (top view) of experimental layout with laser and FTIR systems.

142 Because the probe was inserted directly in the flame above the plants (Fig. 1b) and because
 143 Teflon® melts at ca. 327 °C, the flame gas samples were pumped into the cell / FTIR instrument
 144 via a stainless steel tube that was heated outside for those sections outside the wind tunnel. This
 145 has proven effective at preventing adhesion for nearly all gases except amines (Scharko 2019a).
 146 Gas from further probes was pumped into canisters for offline analysis using gas chromatography.
 147 Sixty-six or seventy-four live plants were distributed within the longleaf pine needles in ceramic
 148 holders. Figure 1a shows the configuration of the fuel bed with instrumentation for *in situ* analysis.
 149 Plant species were prepared on site and samples of dry and live fuel were clipped to determine fuel
 150 moisture content prior to each burn set. The experiments were set under varying fuel bed and
 151 environmental conditions as summarized by Table 1 for the 21 experiments presented in this paper.

152 **Table 1.** Summary of burn schedule for November 2018 studies including burn number, date and time, fuel
 153 description, acquisition method and resolution used for wind tunnel experiments under 1 m s⁻¹ imposed air flow.
 154 Geometric mean flame spread rate = 0.01 m s⁻¹. The FTIR acquisition methods are described in the text.

155

Burn number	Date (2018)	Local ignition time (PDT)	Local finish time (PDT)	Plant species	Acquisition method	Resolution (cm ⁻¹)
76	30-Oct	11:48:01	11:52:00	inkberry	static	0.6
77	30-Oct	14:19:10	14:23:37	fetterbush	dynamic	2.0
78	30-Oct	15:12:30	15:16:33	sparkleberry	static	0.6
79	30-Oct	16:17:00	16:21:10	inkberry	dynamic	2.0
80	31-Oct	9:32:00	9:35:45	sparkleberry	static	0.6
81	31-Oct	10:35:00	10:38:52	fetterbush	dynamic	1.0
82	31-Oct	11:30:30	11:35:15	sparkleberry	static	0.6
83	31-Oct	13:19:00	13:22:58	inkberry	dynamic	1.0
84	31-Oct	14:12:15	14:16:30	fetterbush	static	0.6
85	31-Oct	15:30:30	15:34:24	fetterbush	dynamic	2.0
86	1-Nov	9:30:00	9:33:02	sparkleberry	dynamic	1.0
87	1-Nov	10:40:00	10:42:49	inkberry	dynamic	1.0
88	1-Nov	11:40:00	11:42:59	fetterbush	static	0.6
89	1-Nov	13:35:00	13:38:48	inkberry	static	0.6
90	1-Nov	14:45:00	14:49:47	sparkleberry	static	0.6
92	2-Nov	9:30:00	9:34:05	inkberry	dynamic	0.6
93	2-Nov	10:41:15	10:45:44	fetterbush	dynamic	1.0
94	2-Nov	11:28:15	11:32:28	sparkleberry	static	0.6
95	2-Nov	13:42:45	13:46:17	sparkleberry	static	0.6
97	2-Nov	15:38:38	15:41:40	sparkleberry	dynamic	0.6

156

157 2.2 Instrumentation

158 Gases were extracted from the burns via 3/8" stainless steel tubing, HEPA filtered to eliminate tar
159 and char contamination and pumped into an 8-meter White cell (Bruker A136, 2.2 liter volume)¹
160 housed inside a Bruker Tensor 37 spectrometer (Figure 1c). The extractive probe was placed
161 directly above a plant as close as possible to the foliage. To prevent analyte/tar condensation, both
162 transfer tubing and the gas cell were heated to ~50 °C using heating tape/voltage regulator and a
163 cell heating shroud, respectively. A thermocouple was suspended into the White cell to record the
164 gas temperature for subsequent spectral analysis, with pressure gauge mounted atop the cell. Prior
165 to data collection, the White cell was aligned using the FTIR's Ge/CaF₂ beamsplitter and W-lamp
166 source. Once aligned, these were replaced with a Ge/KBr beamsplitter and mid-IR globar source,
167 along with a mercury cadmium telluride detector, configuring the Tensor 37 to record spectral data
168 from 7500 to 500 cm⁻¹.

169 The FTIR system was tested for leaks, followed by a gas cell path length calibration using purified
170 isopropyl alcohol (IPA - Sigma Aldrich 99.5%). Ten spectra with IPA pressures between 0.6 and
171 10.5 Torr were recorded to 0.1 Torr using an MKS KF15 pressure transducer. The integrated area
172 of the 3515-3290 cm⁻¹ spectral domain (Bruker OPUS 5.5 software) along with recorded
173 temperatures and pressures were used to create a Beer-Lambert plot (Scharko et al. 2019a). Using
174 the integrals from the ten recorded spectra the cell path length was determined to be 6.5 ± 0.2 m.
175 Wavelength calibration of the infrared data was achieved after the fact using a series of 30 water
176 rotational-vibrational lines from the PNNL gas-phase database. (Sharpe et al. 2002; Williams et
177 al., 2013). FTIR interferograms were acquired using double-sided, forward-backward acquisition;
178 these were apodized using a Blackman-Harris 3-Term function and phase corrected with Mertz's
179 method prior to Fourier transformation. **For both acquisition modes (static / dynamic), a single I₀**
180 **reference spectrum at the appropriate resolution was collected by flowing ambient gas into the cell**
181 **at the start of each day to form the single (static) or multiple (dynamic) decadic absorbance spectra**
182 **using Beer's law: - log₁₀(I/I₀). Acquiring such a blank or zero I₀ spectrum effectively accounts for**
183 **any trace VOC emissions from the White cell, wind tunnel, tubing etc.**

184 2.3 Infrared spectral acquisition

¹ The use of trade or firm names in this publication is for reader information and does not imply endorsement by the U.S. Department of Agriculture of any product or service.

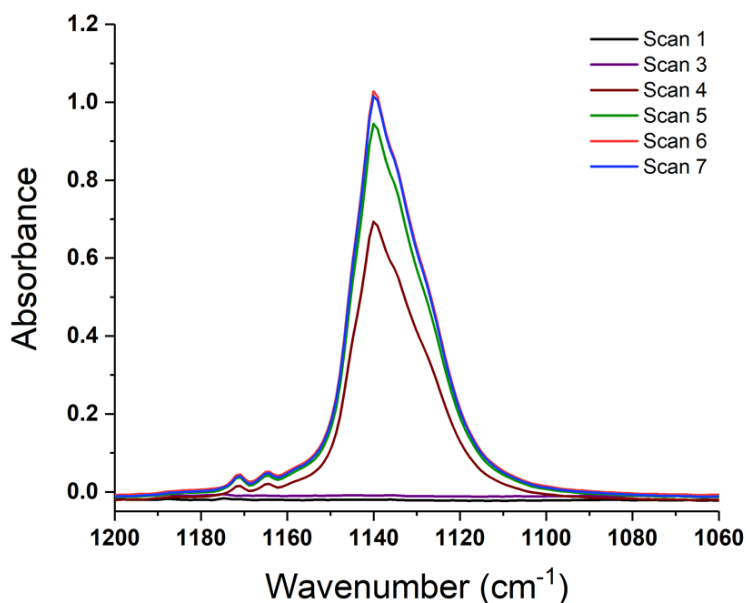
185 Two data acquisition modes were used to analyze the burn gases: an extractive (or static) mode
186 and a dynamic mode. In the extractive mode the gas flowing through the White cell was isolated;
187 the inlet/outlet valves were simultaneously closed such that the emitted gases were isolated in the
188 cell at a desired pressure (ca. 740-700 Torr for high pressures, and 430-400 Torr for lower pressure
189 measurements). The valves were closed just prior to the flame front reaching the probe, attempting
190 to capture pre-combustion phases including evaporation and pyrolysis. The goal of the extractive
191 mode was to obtain a higher fidelity “snapshot” for a given point in time of the burn; more data
192 were averaged longer at higher spectral resolution allowing for detection of more gaseous species
193 with higher sensitivity. (Scharko et al., 2019a). The dynamic mode measurements had fewer scans
194 at lower resolution to capture changing chemical identities/composition corresponding to different
195 fire phases (pyrolysis, flaming combustion, smoldering combustion), achieving temporal
196 resolutions of the order of ca. 1 Hz.

197 Of the 21 burns, 10 were recorded using the static method (Table 1). The static experiment spectra
198 were recorded using the full resolution of the spectrometer (0.6 cm^{-1}), a 2 mm Jacquinot stop and
199 double sided, forward-backward acquisition. Due to the higher resolution and lower light
200 throughput, acquisition time was extended by averaging multiple scans for a full 30 minutes,
201 resulting in vastly improved signal/noise ratios (SNR). For analysis of such complicated gas-phase
202 mixtures, infrared spectral resolutions of 1.0 cm^{-1} or better have been demonstrated to be
203 advantageous (Burling et al., 2010, Akagi et al., 2014, Scharko et al., 2019a). While one goal was
204 to isolate gases to include only the pyrolysis and pre-combustion phases, one vagary of the
205 technique involved the timed closing of the valves relative to arrival of the flame front approaching
206 the inlet. If the valves were shut too early, the captured emissions would consist of only (warmed)
207 ambient gas before onset of thermal degradation of the solid fuel, as opposed to the desired
208 pyrolysis phase. Conversely, if shut too late, flaming, or possibly even smoldering conditions
209 would be sampled.

210 The second method was the dynamic mode whereby the OPUS software was used to continuously
211 collect interferograms throughout the duration of the burn, capturing the chemical compositions
212 associated with different phases, e.g. volatilization, heating, pyrolysis, flaming or smoldering
213 combustion. Fourier transformation of the interferograms occurred after the burns to yield faster
214 acquisition times. The dynamic acquisition mode was used in combination with thermal IR video
215 imaging recorded from above the flame bed to help synchronize spectral acquisition to the various

216 burn phases for a total of 11 burns. Instead of averaging for 30 minutes, the dynamic method
217 allowed for 40-80 continuous interferometer scans (differing on the duration of the burn), and
218 yielded a spectrum every 1.5 s for data taken at 1.0 cm^{-1} resolution, every 0.79 s for data at 2.0 cm^{-1}
219 $^{-1}$ resolution, and every 2.5 s for 0.6 cm^{-1} resolution spectra. Data acquisition began as the flame
220 front encroached upon the extractive probe and continued until the flame had passed. Due to the
221 faster acquisition rate these spectra are significantly noisier than the data collected using the
222 extractive method. To compare results from the static and dynamic modes, fires 87 and 89 will be
223 presented. The 2 m length fuel beds for both experiments 87 and 89 consisted of 1 kg longleaf pine
224 needles with interspersed inkberry plants.

225 For time synchronization it was necessary to quantify the time lag from the time the emissions
226 enter the extractive probe to midpoint in their flow through the White cell. A flow rate test was
227 thus conducted using freon gas, CFC-11 (trichlorofluoromethane) which is comparable in
228 molecular weight to the heavier gases detected by the FTIR. Figure 2 shows such a test of CFC-
229 11 being introduced with spectra recorded every 0.79 s using 2.0 cm^{-1} resolution. The time from
230 introduction of the freon at the extractive probe ($t=0$, scan 0) to first appearance in scan 4 (maroon
231 trace) was 3.2 seconds. The freon spectra had maximized at scan 6 (red trace) for a total $\Delta t = 4.8$
232 s lag from the probe to the instrument. With this information, FTIR time stamped data were then
233 adjusted to reflect the 4.8 second time delay which was used when correlating the spectral data to
234 the visual and thermal IR video images.



235

236 **Figure 2:** Dynamic spectra recording introduction of CFC-11 from extractive probe to gas cell. Scan 0 (not
237 shown) represents start of spectral acquisition/freon release near probe. Spectra produced every 0.79 s. First
238 observation of freon occurs with scan 4; maximum absorbance of CFC-11 and stabilization occurs at scan 6.

239 2.4 Spectral Analysis

240 A combination of software was used for the post-acquisition spectral analysis and confirmation of
241 the species observed during the campaign. The MALT5 software (Griffith, 2016) utilizing both
242 HITRAN line-by-line data (Gordon et al., 2017) as well as the PNNL 50 °C gas-phase reference
243 spectra (Kochanov, 2019; Johnson et al., 2006, 2010) as input libraries was used to identify and
244 quantify vapor-phase chemicals in the spectra. Spectra were compiled into parameter files and
245 analyzed by the MALT software using parameters including pressure, temperature, pathlength,
246 resolution, as well as estimated initial values for chemical mixing ratios. The software generates a
247 spectrum to simulate the measured spectrum, adjusting mixing ratios until the residual between
248 the simulated and measured spectra is minimized. To confirm the species were actually present,
249 each spectrum generated by MALT was input to OPUS and subtracted from the measured
250 spectrum; the target compound was purposefully omitted from the subtraction process to visually
251 inspect if the omitted compound was in fact present (see e.g. Figure 5).

252 3. Results and Discussion

253 3.1 Analysis of Static Spectra

254 Ten spectra were recorded from different burns using the static mode with the gas cell valves
255 closed simultaneously; gases were sampled prior to arrival of the flame front (Figure 1c). A total
256 of 29 compounds were detected and confirmed using MALT5 and OPUS 5.5. Along with CO,
257 CO₂ and nitrogen compounds, the gas-phase species are largely lightweight hydrocarbons (HCs),
258 volatile organic compounds (VOCs) and oxygenated volatile organic compounds (OVOCs). Table
259 2 provides a summary of all compounds observed during the static measurements and is broken
260 down into subcategories of chemical classes by rows labeled a-e, with ambient gases such as CO
261 and CO₂ in group a, alkanes and alkenes in group b, alcohols, aldehydes and carboxylic acids in
262 group c, aromatic species in group d, and N-bearing compounds in group e. The benefits of the *in*
263 *situ* laboratory static measurements were controlled gas sample collection with FTIR analysis and
264 longer scan times for increased SNRs at higher spectral resolution. Valves were shut before the
265 flame front arrived allowing for minimal mixing of air and flame gases near the extractive probe.
266 In this manner the targeted pyrolysis phase was likely to be sampled with a greater mole fraction

267 rather than that of the combustion phase. The gases listed in Table 2 have previously been
268 observed in smoke in either field or laboratory settings, and some have been linked to pyrolysis
269 (Scharko, 2019a,b; Burling et al., 2010, 2011; Christian et al., 2003, 2004; Gilman et al., 2015;
270 Goode et al., 1999, 2000; Hatch et al., 2017; Selimovic et al., 2018; Stockwell et al., 2014;
271 Yokelson et al., 1996, 1997; Akagi et al., 2013, 2014; Alves et al., 2010; Hurst et al., 1994a, b;
272 Karl et al., 2007; Paton-Walsh et al., 2010). Compounds associated with the pyrolysis phase and
273 observed in several of the static measurements include acetic acid, ethene (C₂H₄), allene, 1,3-
274 butadiene, acetaldehyde, formic acid, formaldehyde, acrolein, benzene, furan, furaldehyde,
275 naphthalene and phenol.

276 As seen in Table 2, ammonia gas (NH₃) was also detected at fairly low mixing ratios in the
277 laboratory scale experiments, which had previously not been detected in the Ft. Jackson field
278 study: The lack of NH₃ detection in those studies was ascribed to the known adsorptivity of the
279 compound as it may have adhered to either the transfer canister walls, the extractive probe, or the
280 White Cell, all at ambient temperatures as used in those studies (Scharko et al., 2019; Roscioli et
281 al., 2015; Stockwell et al., 2014; Yokelson et al., 2003; Neuman et al., 1999). Adhesion losses
282 were minimized in the present experiments by a) measuring the gas parcel directly without storage
283 and b) heating transfer lines and gas cell to ~55 °C.

284 **Table 2.** Mixing ratio of chemicals from spectra collected using the static acquisition method. Burns are labeled
285 by number and plant species. Compound mixing ratios are reported in ppm (with the exception of H₂O and CO₂
286 reported as percents) and categorized by (a) background ambient compounds, (b) simple hydrocarbons, (c)
287 oxygenated organic compounds, (d) aromatics and furans, and (e) N-bearing species.

		Burn 76	Burn 78	Burn 80	Burn 82	Burn 84	Burn 88	Burn 89	Burn 90	Burn 94	Burn 95
		inkberry	sparkleberry	sparkleberry	sparkleberry	fetterbush	fetterbush	inkberry	sparkleberry	sparkleberry	sparkleberry
a	% H ₂ O	1.24	1.05	3.23	2.03	3.54	3.08	3.46	1.82	6.21	4.10
	% CO ₂	0.06	0.09	2.06	0.48	1.51	2.06	1.36	0.34	4.60	2.08
	CO	1.45	3.90	808	192	1089	1057	391	160	7506	2651
	N ₂ O	0.35	0.34	1.21	0.50	1.28	1.79	0.44	0.41	3.22	1.78
b	CH ₄	2.27	2.21	45.3	10.7	54.5	50.3	15.4	11.3	682	198
	C ₂ H ₂	0.01	0.06	23.8	4.52	23.4	23.2	8.82	5.62	351	96.5
	C ₂ H ₄	0.07	0.05	29.3	7.05	39.9	39.3	9.66	6.52	452	133
	C ₂ H ₆			0.83			2.76		4.00E-04	24.2	6.29
	C ₃ H ₆			4.02	0.99	5.55	5.48	0.75	0.77	61.3	18.1
	allene	0.17		0.64	0.29	1.12	1.21	0.25	0.12	8.69	2.30
	1,3-butadiene			1.63	0.37	1.98	2.07	0.26	0.43	28.1	7.57
	isobutene			0.75		0.74	0.52			3.16	1.07
	isoprene			1.78	0.39	1.72	1.43	0.31	0.32	11.7	4.22
	CH ₃ OH	0.89	0.24	6.81	1.53	6.92	9.44	1.66	0.93	42.3	18.0
c	C ₂ H ₅ OH	1.37									
	acetic acid	0.07		5.93	3.55	13.4	13.8	11.0	2.49	13.4	9.62
	formic acid			15.9	5.14	32.35	35.3	9.20	3.64	130	73.6
	acetaldehyde			5.87	1.69	7.62	8.65	1.51	0.94	73.6	22.6
	acrolein			2.59	1.29	3.99	4.35	0.98	0.00	26.0	9.53
	crotonaldehyde			1.51	0.54			0.73	0.17	9.97	5.64
	formaldehyde		0.08	13.6	4.31	21.3	22.5	5.41	3.33	114	52.8
	benzene			4.08	2.23	5.19	4.24	1.93	1.48	61.3	18.6
d	furan			0.75		0.39	0.54			3.07	1.16
	furfural			0.65	0.06				0.13	3.34	1.24
	naphthalene			4.48	1.06	3.60	4.80	3.40	0.82	14.6	1.42
	phenol			0.90	0.30	1.36	1.63	1.75	0.37	2.19	1.63
e	NH ₃	0.10	0.29	0.19	1.29	1.79	0.88	1.08	0.41	0.58	0.57
	HCN			5.84	2.19	8.25	6.94	3.36	1.69	64.2	21.0
	HNCO			1.89	0.67	2.61	2.94	1.27	0.70	5.37	1.98
	HONO		0.11	9.40	2.53	9.72	12.7	8.92	1.75	26.9	11.3

288

289

290 When comparing the RFL laboratory scale experiments to the 2018 Ft. Jackson field scale
291 experiments (Table 3), it is evident that field scale values via the static mode are greater than those
292 of the laboratory, even though the laboratory experiment attempted to replicate Ft. Jackson fuel
293 beds and scenarios. In most cases, a comparison of compounds found in the RFL laboratory burns
294 and the Ft. Jackson 2018 field burns finds Ft. Jackson mixing ratios approximately 4 to 10x greater
295 than those of the RFL 2018 tunnel data. Field scale measurements typically yield more emissions
296 than experiments conducted in the laboratory (Yokelson, 2013; Scharko, 2019b, Weise et al.
297 2015). However, while the mixing ratios may differ or be larger/smaller, the information
298 describing the composition of the mixture is relative in nature and is contained in log-ratios of the
299 various gases. But analysis of the data as compositional data (Aitchison 1986) is beyond the scope
300 of the present paper. Table 3 displays the minimum and maximum mixing ratio values in ppm for
301 five compounds from the Ft. Jackson studies presented in Scharko et al. (2019a) versus the present
302 RFL laboratory results. Of the five species compared, acetaldehyde, acrolein, and allene all follow
303 the trend of having Ft. Jackson results being significantly higher than the RFL studies by a factor

304 of ~4. Naphthalene, a polycyclic aromatic hydrocarbon (PAH) was the only exception to this trend,
 305 having comparable mixing ratio values in the two studies. This anomaly could be attributed to one
 306 of naphthalene’s pyrolysis formation route as suggested by Fairburn et al., where a single ringed
 307 aromatic compound undergoes a Diels-Alder reaction of an alkene (Fairburn et al., 1990; Liu et
 308 al., 2017). Of the four compounds compared, naphthalene is the only one to be derived from a
 309 secondary reaction, whereas acetaldehyde and acrolein are derived directly from the pyrolysis of
 310 cellulose (Stein et al., 1983), while allene is a compound known to be a precursor of aromatic
 311 compounds and soot (Frenklach et al., 1983, 1988). As noted, most compounds detected in the
 312 RFL laboratory studies yielded ~4 to 10x lower mixing ratios compared to the field scale studies
 313 at Ft. Jackson. Along with naphthalene, however, acetic acid, formaldehyde, isoprene and
 314 isobutene were also found to have comparable mixing ratios to those reported in the Ft. Jackson
 315 studies. This could be due to the four compounds being products of secondary reactions, or
 316 fragmentation, of species such as lignin, xylan and glucomannan (Collard and Blin, 2014). It
 317 should be noted that of the five novel compounds detected in Scharko et al. (2019b), only four
 318 were detected in these laboratory scale experiments. Methyl nitrite was not observed (Table 3).
 319 This is attributed to the field experiment being on the Ft. Jackson base where there is known to be
 320 unexploded ordinance (Scharko et al., 2019b) or possibly due to lower concentration levels that
 321 are below the detection limits of the present laboratory-scale experiment.

322 **Table 3.** Calculated minimum and maximum mixing ratios (ppm) for the 10 canister measurements taken at the
 323 Ft. Jackson field measurements (Scharko et al., 2019) along with the minimum and maximum mixing ratios
 324 (ppm) for the 10 static measurements during the RFL laboratory experiment of acetaldehyde, acrolein, allene,
 325 methyl nitrite and naphthalene.

Target Compound	Ft. Jackson calculated mixing ratio (ppm)		RFL calculated mixing ratio (ppm)	
	min	max	min	max
acetaldehyde	34.5	264.8	0.94	73.6
acrolein	14.7	125.7	0.98	26
allene	2.2	37.8	0.12	8.69
methyl nitrite	2.3	21	-	-
naphthalene	1.4	19.9	0.86	14.6

326
 327 It is clear that the static method as deployed was not perfect at either isolating strictly the pyrolysis
 328 phase gases or capturing extremely high fractions of combustion gases. The method relied heavily
 329 on valves being closed prior to the flame front using visual cues as opposed to using other

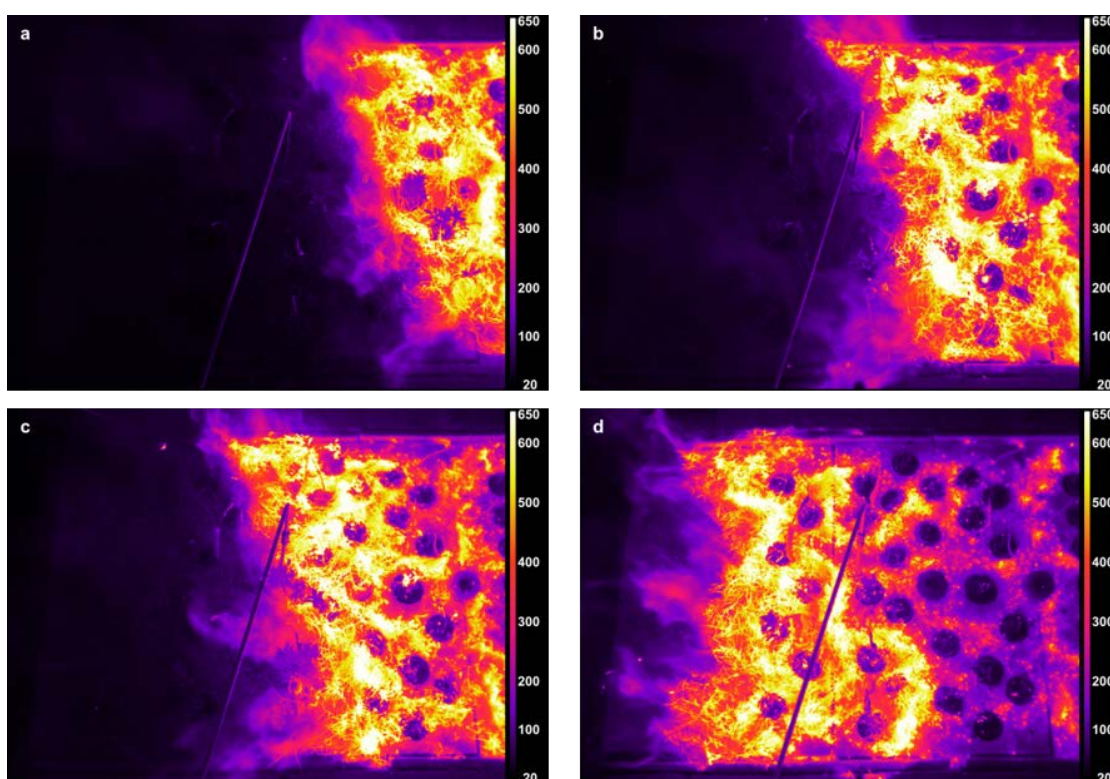
330 techniques, e.g. thermal IR. While not readily visible to the human eye, radiant and convective
331 heating (as determined by Background-Oriented Schlieren measurements - Aminfar et al 2019)
332 occurred well in advance of the flame front, suggesting this as a possible alternate visualization
333 of pyrolysis gas release (Aminfar 2019). In any case, there is a narrow temporal window for the
334 pre-combustion phase making the valve-close time extremely important. For example, spectra
335 from burns 76 and 78 show largely the detection of only ambient air compounds indicating the
336 valves were closed too early. Conversely, in other samples there is clearly some mixing of both
337 upstream and downstream air before the gas enters the extractive probe. Despite the shortcomings
338 of the static method most of the attempts to obtain pre-combustion gases were successful as
339 evidenced in part by the chemical composition of the isolated gases.

340

341 *3.2 Spectral-Thermal Correlation to Isolate Pyrolysis Phase*

342 Dynamic IR data and visual image acquisition proved advantageous to resolve the different phases
343 of the experiments (e.g. pyrolysis, flaming combustion, smoldering combustion). This was
344 important since MCE is a function of the gas composition and is not unique to phase (i.e., the same
345 value of MCE results if the same relative amounts of CO and CO₂ are observed, whether in the
346 pyrolysis, flaming or smoldering combustion phases). MCE, defined as $\Delta\text{CO}_2/(\Delta\text{CO} + \Delta\text{CO}_2)$,
347 has many times been used to distinguish phases of combustion, namely flaming vs. smoldering
348 although Ward and Radke (1993) recommended combustion efficiency as the preferred descriptor
349 of the combustion system. MCE has not been used to identify pyrolysis nor should it be for the
350 non-uniqueness described previously. Recent studies have introduced more sophisticated
351 techniques to analyze smoke emissions data with compositional data methods (Weise et al. 2020).
352 However, since primary and secondary pyrolysis occurs both prior to and after the onset of
353 combustion or oxidation, methods such as the MCE are not appropriate. We were not able to use
354 the metric suggested by Sekimoto et al. (2018), namely high temperature vs. low temperature
355 pyrolysis as determined from the acetylene-to-furan ratio due to weak furan signals in the present
356 study due to shortened scan times. The analysis was further exacerbated because furan's strongest
357 vibrational band, the ν_{19} vibrational band near 745 cm⁻¹, corresponding to the C-H out-of-plane
358 bend (Shimanouchi, 1972), was obscured by saturated carbon dioxide lines and thus MALT was
359 not able to generate a satisfactory fit for this microwindow.

360 The pre-flame arrival gases were identified by either of two methods: The first method involved a
361 simple time subtraction of 4.8 s from the recording of the infrared spectrum time stamp and
362 associating that time to the corresponding visual and FLIR thermal infrared video images (Fig. 3).
363 This provided a relatively accurate verification that the gases being investigated were emitted prior
364 to the onset of combustion as seen in Table 4. The second method used the FTIR spectra directly:
365 demarcations for the flame front were denoted by the maximal value obtained for both CO and
366 CO₂ concentrations, i.e. greatest fraction of gas from the combustion phase. From this value the
367 FTIR's scans were selected for pyrolysis corresponding to the ~10 seconds before arrival (~0.1 m
368 distance) of the flame front.



369
370 **Figure 3.** Burn 87 inkberry on longleaf pine needle fuel bed – FLIR thermal imaging for burn progression.
371 (a) frame corresponding to FTIR scan 5 signaling the pre-combustion phase, (b) frame corresponding to
372 FTIR scan 16, flame front nearing sample probe, (c) frame corresponding to FTIR scan 21, inkberry bush
373 consumed by flame, (d) frame corresponding to FTIR scan 44, flame front has passed the probe. Dark
374 circles are ceramic plant holders.

375 The FTIR time-resolved scans (including derived chemical mixing ratios) synchronized to the RFL
376 time-stamped thermal IR temperature images provide insight into the chemical composition of
377 each burn. As an example, Table 4 pairs data from the two systems for Burn 87. FTIR scan number,
378 FTIR time stamp, RFL FLIR recorded temperature near the extractive probe, and a selection of

379 chemical concentrations are shown. The table demonstrates that spectral data for FTIR scans 0-8
380 saw no significant detections above ambient levels as corroborated by the FLIR images displaying
381 temperatures range from 40-80 °C (see Table 4 and Figure 3a); the extractive probe is still in the
382 low temperature region. The gradual increase in mixing ratios for most compounds (excluding
383 ammonia, which is primarily a smoldering gas) begins after FTIR scan 9. The magenta and orange
384 colored domains seen in Figure 3b indicate the encroaching flame front and a rise in thermal
385 temperatures. The frames corresponding to FTIR scans 16-19 display IR temperatures between
386 175 and 220 °C. In this temperature range compounds associated with the pyrolysis phase such as
387 acetaldehyde, acetic acid and allene (shown in Table 4) are not only manifest in the IR spectra, but
388 their mixing ratios rise rapidly. Shortly thereafter the greatest mixing ratios of CO₂ occur at scans
389 20 through 22, indicating the flaming stage; this is corroborated by thermal IR video of the inkberry
390 plant beginning to be fully consumed in flames (Fig 3c). As the flame front progressed down the
391 tunnel, temperatures near the plant holder began to drop with the onset of the smoldering phase as
392 indicated by lower mixing ratios as well as the thermal IR visual seen in Fig. 3d. [We note in
393 Figure 3 that the temperature directly near/above the holders is much cooler due to minimal duff
394 cover and the plants being green.] The video stopped recording at scan 48, when the flame reached
395 the end of the fuel bed although the FTIR continued to collect interferograms to monitor
396 smoldering from the fire.

397
398 **Table 4:** Burn 87 inkberry amongst pine needle fuel bed FTIR scan summary synchronized to FLIR temperature data.
399 Scan number, FTIR time stamp, along with FLIR video emissions temperature at extractive probe accounting for time
400 delay and mixing ratios from carbon dioxide (CO₂), carbon monoxide (CO), ethene (C₂H₄), acetic acid (CH₃COOH),
401 formaldehyde (HCHO), acetaldehyde (CH₃CHO), and phenol (C₆H₆O).

	FTIR Scan Number	FTIR time stamp	4.8 s Delayed FLIR Video Time Stamp	FLIR temperature at inlet (°C)	CO ₂ (ppm)	CO (ppm)	C ₂ H ₄ (ppm)	CH ₃ COOH (ppm)	HCHO (ppm)	CH ₃ CHO (ppm)	C ₆ H ₆ O (ppm)
	scan 0	10:41:23.69	10:41:18.89	41.4	1548	49.5	2.4	0.0	0.6	-	-
	scan 1	10:41:25.20	10:41:20.40	44.2	1912	74.5	1.9	1.7	0.9	-	-
	scan 2	10:41:26.70	10:41:21.90	51.0	1562	63.7	2.3	1.1	0.3	-	-
Ambient	scan 3	10:41:28.21	10:41:23.41	54.9	1290	58.4	1.1	0.5	0.5	-	-
	scan 4	10:41:29.71	10:41:24.91	53.4	1882	63.1	1.2	1.2	0.8	-	-
	scan 5	10:41:31.21	10:41:26.41	63.2	1946	57.0	1.5	1.1	0.4	-	-
	scan 6	10:41:32.72	10:41:27.92	72.8	3811	102	4.7	1.8	1.2	-	-
	scan 7	10:41:34.22	10:41:29.42	77.6	4722	138	2.7	1.9	1.5	-	-
	scan 8	10:41:35.73	10:41:30.93	86.2	3553	109	0.9	2.2	1.4	-	-
Volatilization + Pyrolysis	scan 9	10:41:37.23	10:41:32.43	116.9	2957	97	1.0	2.4	0.7	-	-
	scan 10	10:41:38.73	10:41:33.93	132.1	3360	138	1.8	2.8	1.2	1.4	-
	scan 11	10:41:40.24	10:41:35.44	115.7	7476	246	4.2	2.6	3.6	0.0	-
	scan 12	10:41:41.74	10:41:36.94	121.3	10274	291	6.2	9.0	4.8	4.2	0.7
	scan 13	10:41:43.25	10:41:38.45	183.3	10890	391	11.4	11.5	7.1	1.1	1.6
	scan 14	10:41:44.75	10:41:39.95	159.4	11833	635	23.5	14.5	13.5	3.3	1.5
	scan 15	10:41:46.25	10:41:41.45	163.8	16080	1214	48.5	16.8	28.7	7.2	1.5
	scan 16	10:41:47.76	10:41:42.96	176.9	25757	2217	95.3	16.3	54.4	17.6	1.0
	scan 17	10:41:49.26	10:41:44.46	181.3	31856	2915	129	14.4	70.5	24.0	1.4
	scan 18	10:41:50.77	10:41:45.97	220.1	41291	2878	260	13.1	92.6	34.5	1.4
	scan 19	10:41:52.27	10:41:47.47	219.0	61166	8228	435	12.3	121	44.3	2.1
Flaming Combustion	scan 20	10:41:53.77	10:41:48.97	296.1	79332	11354	747	13.1	178	80.7	2.9
	scan 21	10:41:55.28	10:41:50.48	261.7	54381	9729	1167	17.6	255	140	4.7
	scan 22	10:41:56.78	10:41:51.98	456.1	64077	12954	1025	15.3	185	103	6.0
	scan 23	10:41:58.29	10:41:53.49	429.9	41495	8620	530	15.4	123	63.3	6.3
	scan 24	10:41:59.79	10:41:54.99	516.5	25879	3453	257	15.5	74.5	33.9	6.8
	scan 25	10:42:01.29	10:41:56.49	514.5	15965	3110	116	15.1	45.7	19.6	6.8
	scan 26	10:42:02.80	10:41:58.00	460.1	11819	2416	53.2	15.6	35.2	12.0	5.6
	scan 27	10:42:04.30	10:41:59.50	453.7	8566	1875	36.6	14.7	27.4	6.9	5.2
	scan 28	10:42:05.81	10:42:01.01	448.0	5795	1320	14.5	13.2	21.8	3.0	5.6
	scan 29	10:42:07.31	10:42:02.51	440.2	5235	1302	11.0	14.6	20.0	5.1	4.5
	scan 30	10:42:08.81	10:42:04.01	484.7	3626	916	5.8	15.1	15.0	5.2	4.2
	scan 31	10:42:10.32	10:42:05.52	470.4	2368	570	3.3	11.5	11.1	2.7	3.8
	scan 32	10:42:11.82	10:42:07.02	497.5	1636	377	1.6	10.8	9.4	0.3	3.7
	scan 33	10:42:13.33	10:42:08.53	477.4	1684	399	1.0	9.2	8.8	2.1	3.4
	scan 34	10:42:14.83	10:42:10.03	450.1	1986	519	0.9	10.4	9.5	-1.5	3.0
Smoldering Combustion	scan 35	10:42:16.33	10:42:11.53	397.9	1968	518	0.7	9.9	9.3	2.8	3.2
	scan 36	10:42:17.84	10:42:13.04	410.2	1901	495	1.4	9.6	8.8	0.9	2.8
	scan 37	10:42:19.34	10:42:14.54	401.6	1936	516	1.5	9.2	9.4	0.0	2.7
	scan 38	10:42:20.85	10:42:16.05	358.3	1935	513	1.6	9.0	9.5	1.1	2.8
	scan 39	10:42:22.35	10:42:17.55	341.8	1753	439	1.8	9.7	8.9	1.1	2.3
	scan 40	10:42:23.85	10:42:19.05	320.6	1438	345	1.4	10.4	8.3	-0.5	2.9
	scan 41	10:42:25.36	10:42:20.56	305.9	1224	277	-0.1	10.9	7.4	1.4	2.8
	scan 42	10:42:26.86	10:42:22.06	295.0	1377	324	1.4	11.6	8.2	-2.0	2.4
	scan 43	10:42:28.37	10:42:23.57	272.5	1629	411	1.1	11.8	8.4	0.3	2.4
	scan 44	10:42:29.87	10:42:25.07	258.3	1366	325	0.8	12.8	7.8	2.5	2.7
	scan 45	10:42:31.37	10:42:26.57	260.1	1059	212	0.4	11.9	6.7	3.4	2.7
	scan 46	10:42:32.88	10:42:28.08	238.5	1037	212	0.8	13.1	7.1	0.5	2.3
	scan 47	10:42:34.38	10:42:29.58	223.9	1094	236	0.9	14.4	6.7	1.1	1.2
	scan 48	10:42:35.89	10:42:31.09	226.7	1117	248	1.2	13.1	7.0	-0.4	2.7

402

403

404 As stated, a second method was also used to analyze/corroborate the different stages of the burn,

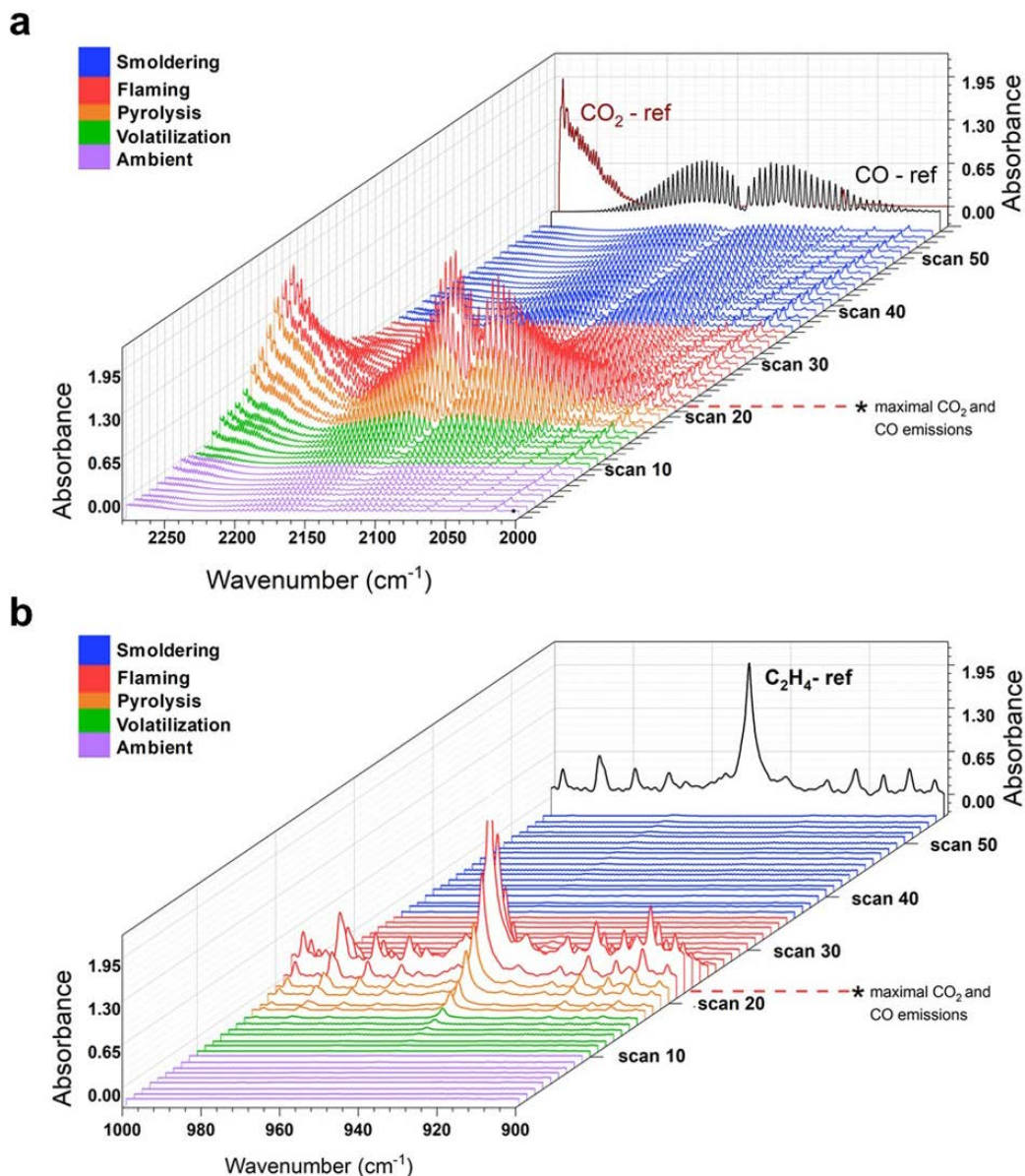
405 whereby mixing ratios of CO₂, CO and C₂H₄ were analyzed to find their burn maxima (Viatte et

406 al., 2015). The CO₂ elevated mixing ratios (esp. relative to CO) are associated with the hottest,

407 flaming stage of biomass burns (Yokelson et al., 1996). To temporally isolate the flaming stage,

408 the MCE criteria was employed and values of 88-95% indicative of smoldering were found for the
409 region. Having identified the flaming stage, the pyrolysis stage was estimated by subtracting 6-8
410 seconds from that spectrum with maximal CO/CO₂ emissions, corresponding to ~4 FTIR scans (at
411 1 cm⁻¹ resolution). The agreement between the two methods was quite good and helped to
412 demarcate the stages as seen in Table 4.

413
414 Figure 4 displays the infrared spectral progression of Burn 87, longleaf pine needles with inkberry,
415 bed at 1.0 cm⁻¹ resolution looking at two different spectral regions. The CO (and CO₂) profiles are
416 seen in Fig. 4a. Noted on the z-axis is scan 22; scans 20-22 are the time frames where maximal
417 CO₂ and CO emissions were observed; the region is also denoted by red spectral traces. Once the
418 flaming stage had been identified, the pyrolysis phase was then demarcated; in the pyrolysis phase
419 CO was evident (partially from upwind mixing) and was beginning to significantly increase; the
420 stage is indicated by orange traces (scans 16-19) in Figure 4. Other stages assigned were noted as
421 the pre-flame stage where ΔCO and ΔCO₂ were near zero in the FTIR data and are seen as scans
422 0-8 with purple traces. Blue traces correspond to the smoldering phase of combustion, where CO₂
423 mixing ratios decreased, the flame front had passed the extractive probe and MCE values were on
424 the order of 85-75%. The spectral profile and mixing ratios of ethene (C₂H₄) were also used to
425 evaluate the time-resolved FTIR data. (Johnson et al. 1993) This lightweight hydrocarbon is a
426 product of primary pyrolysis and if detected can be used to determine certain stages of the burn
427 (e.g. Yang et al., 2007). Figure 4b displays primarily the ν₇ band of ethene at 949.4 cm⁻¹
428 (Shimanouchi, 1972). Ethene reached its maxima mixing ratio at scan 22 (red traces) before it
429 quickly disappeared, being a pyrolysis gas that was oxidized by the flame. It was first seen to
430 appear as early as scan 13 (green traces) but became clearly evident in scan 16 (orange traces,
431 pyrolysis phase) and continued to grow. The rapid disappearance of C₂H₄ upon combustion is
432 similar to that of formaldehyde and acetaldehyde (Table 4) whose concentrations also dropped
433 after scan 23, but the disappearance is juxtaposed with acetic acid whose values remained
434 ~constant throughout the flaming and smoldering phases. As seen in the IR data, the C₂H₄ gas
435 signal corroborated that ethene is a key product of the primary pyrolysis phase. Other compounds
436 showing significant signals in this time domain and described as pyrolysis gases include acrolein
437 and allene. (Scharko 2019a; Akagi et al., 2013; Frenklach et al. 1983, 1988; Stein et al., 1983;
438 Koss et al., 2018; Brilli et al., 2014).



439
 440 **Figure 4.** Burn 87, inkberry with longleaf pine needles: a) CO and CO₂ spectral profile from 2250-2000 cm⁻¹.
 441 Purple traces indicate the ambient stage, green and orange traces indicate the pre-combustion/pyrolysis stage,
 442 red spectral traces indicate the flaming stage and blue traces indicate smoldering. b) Largely C₂H₄ spectral
 443 waterfall plot from 1000-900 cm⁻¹ with accompanying C₂H₄ reference spectrum as black trace.
 444

445 The two methods to determine the pyrolysis, flaming, combustion and smoldering phases yielded
 446 congruent results: The isolated burn stages determined from method one, in which FTIR gas-
 447 phase data were synchronized to the FLIR thermal imaging, and from method two, using the FTIR
 448 time-resolved data only, were found to be virtually identical. This is evidenced by linking the scans
 449 determined to be in the pyrolysis phase (scans 16-19) using method two as seen in Fig. 4, with the
 450 temperature data recorded by the FLIR using method one and seen in Table 4. For these scans,

451 the temperature profile ranges from 175-220 °C, corresponding to temperatures associated with
452 first stages of pyrolysis.

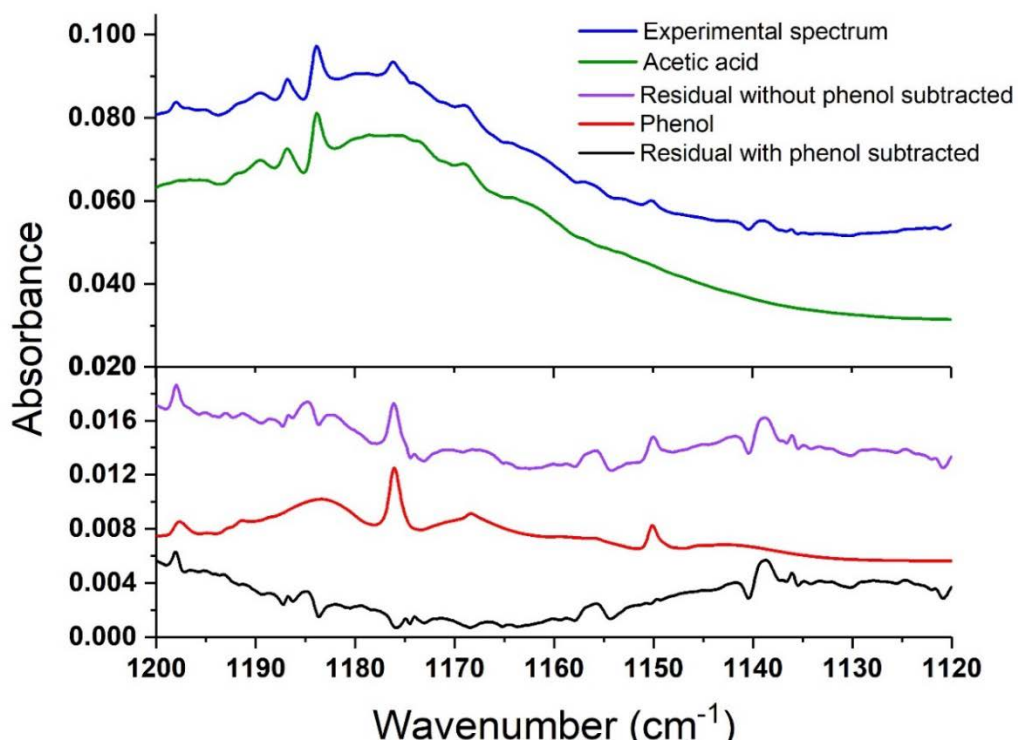
453 For most analytes biomass burning gas mixing ratios, the concentration values observed at the
454 peak of the dynamic measurements values were significantly greater than for the concentrations
455 recorded in the static measurements. The dynamic experiments were of course carried out for the
456 duration of the burn, whereas the static burns (in an effort to characterize pre-combustion phases)
457 attempted to isolate a specific time when the pyrolyzate concentrations were maximized.
458 Analyzing the data using the dynamic technique allowed for confirmation of certain compounds
459 such as naphthalene, allene, acetaldehyde, and acrolein as compounds that appeared during the
460 pyrolysis phase. These compounds, which have been previously detected as pyrolysis gases using
461 FTIR for field plot burns, (Scharcko et al. 2019) were again observed during these laboratory scale
462 tests and in almost all cases appeared before the flame front encroached on the sampling probe.

463 *3.3 Dynamic Detection of Phenol in the Pre-combustion Through Smoldering Stages*

464 In the present study phenol (C₆H₆O) was detected during several burns; its origin ascribed to the
465 pyrolysis of lignin(s) (Kibet et al. 2012, Hawthorne et al. 1989) and has been mostly observed
466 using other techniques such as gas chromatography mass spectrometry (GC-MS). (Saiz-Jimenez
467 et al. 1986) Phenol and phenolic compounds are also known to contribute to the formation of
468 secondary organic aerosols (Yee et al., 2013). It has been observed in simple pyrolysis
469 experiments, emanating from both pine and spruce species (e.g. Saiz-Jimenez and De Leeuw,
470 1986, Ingemarsson et al., 1998). In addition to simply pyrolytic emissions, phenol has also been
471 identified as a common component of tar as a pyrolysis product. In biomass burning, phenol has
472 been observed using both FTIR and other methods, (Gilman et al. 2015, Yokelson et al. 2013), e.g.
473 proton-transfer mass spectrometry (PTR-MS) and GC-MS. In 2013 phenol was detected in a
474 closed cell, airborne FTIR field experiment but not in an open-path FTIR lab experiment
475 (Yokelson et al. 2013). The absence of C₆H₆O in the lab experiment was attributed to the lack of
476 consumption of rotten wood as fuel. In those studies, airborne phenol emissions measured in the
477 field with closed-cell FTIR were also noted as being 2 to 4x greater than the phenol emissions
478 captured by PTR-MS in the laboratory.

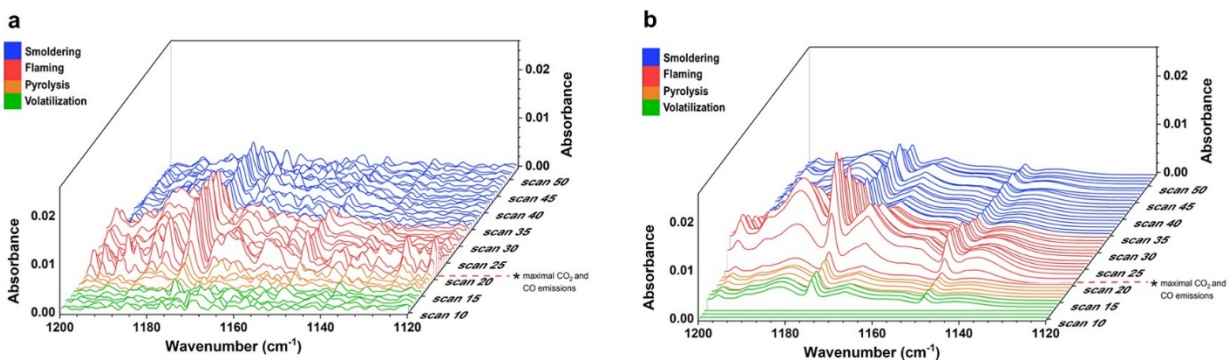
479 Compositional analysis of inkberry, fetterbush, and longleaf pine needles used in the present study
480 showed that the fuels contained 23 to 30 percent structural lignin in the foliage and 3 to 9 percent

481 phenols (Matt et al 2020). Note that none of the fuels in the wind tunnel experiments or the bench-
482 scale experiments contained rotten wood. In the present experiments, phenol was detected in 8 of
483 the 10 static measurements (recall that two of the static measurements only showed ambient gases
484 due to early closure of the valves). Figure 5 demonstrates the static spectrum from Burn 89,
485 corresponding to the burning of longleaf pine with inkberry. Seen in Fig. 5 are the experimental
486 spectrum (blue trace) and also the reference spectrum of acetic acid (green trace). After subtraction
487 of the CH_3COOH vapor spectrum, the residual contained two small peaks which were readily
488 identified as phenol vapor via the ν_{15} vibrational band near 1176.2 cm^{-1} , as well as the ν_{16} band at
489 1150.2 cm^{-1} (Keresztury et al., 1998). The phenol reference spectrum from the PNNL spectral
490 library (red trace) was then subtracted from that residual (purple trace) with an overall residual
491 that is mostly noise (black trace). [For the dynamic spectra the process is repeated for each of the
492 individual spectral time slices, represented by scan number using the concentration of phenol
493 determined by the MALT program.] To confirm the spectral analysis, in each case the mixing ratio
494 calculated by MALT was converted to a spectrum by multiplying by the appropriate concentration
495 path length factor; the predicted spectrum was visually compared to the actual data.



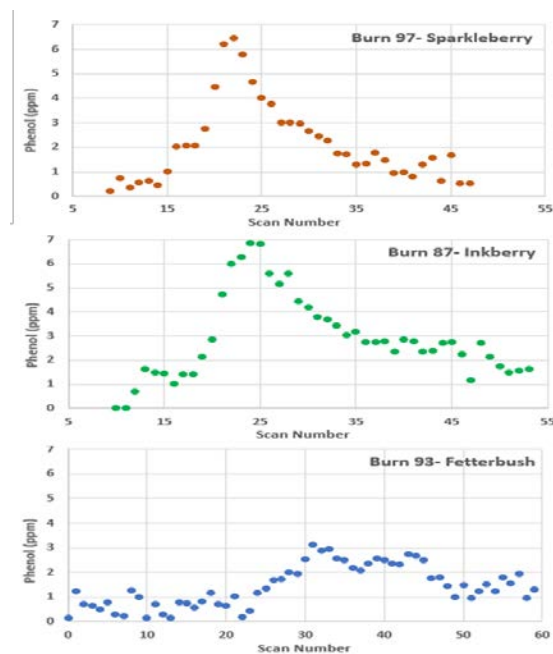
496
497 **Figure 5.** Static spectrum obtained from Burn 89 (1 kg longleaf pine needles with inkberry). The blue trace
498 is the FTIR experimental spectrum, the green trace the reference spectrum of acetic acid, the purple trace
499 the residual after acetic acid subtraction, the red trace the reference spectrum of phenol and the black trace
500 residual after phenol optimization/subtraction.

501 Phenol was also detected using the dynamic method and Figure 6 displays a series of dynamic
 502 spectra recorded for Burn 87. The spectra in the left frame (a) are individual spectra after the acetic
 503 acid (CH_3COOH) spectral component has been subtracted from the spectrum for each time slice,
 504 all recorded at 1.0 cm^{-1} resolution with 54 total measurements recorded at $\Delta t=1.5$ seconds. While
 505 the spectral noise is still significant, the presence of phenol peaks, particularly the ν_{16} Q-branch at
 506 1176.5 cm^{-1} and the ν_{15} peak at 1150.2 cm^{-1} , are evident. Optimization for the phenol mixing ratio
 507 in each spectrum allowed for its calculation in individual time slices and the derived phenol-only
 508 spectra are presented as a waterfall plot in the right frame (b). The first clear evidence of phenol is
 509 seen in scans 14 to 18, before reaching a maximum concentration of 6.9 ppm in scan 24; this is
 510 observed in the right frame of Figure 6, coinciding approximately with maximal CO_2 concentration
 511 (scan 22), indicating the greatest ratio of smoke/ambient air in the gas cell.



512
 513 **Figure 6.** Burn 87 –longleaf pine needles with inkberry fuel bed during dynamic mode. Measured and
 514 scaled burn spectra showing the progression of phenol during the time resolved study. Acetic acid and
 515 water spectral features have been removed in Frame a) with the phenol-only derived mixing ratio spectra
 516 in Frame b.
 517 Figure 6 displays the rapid increase of phenol vapor due to the approaching flame front from scan
 518 14 ($t = 22.5$ s) to its maximal mixing ratio in scan 24 ($t = 36$ s) followed by a longer gradual phenol
 519 decay with time. This can be juxtaposed with the ethene mixing ratios (seen in Figure 4) that fall
 520 to nearly zero with the onset of combustion; the ethene is consumed by the flame propagation.
 521 Prior to scan 14 in Figure 6b, minimal phenol is observed relative to the noise level and are thus
 522 fit as zero concentration. Phenol contributions for scans 16-19 can be associated with the pyrolysis
 523 phase of the burn and not combustion. Phenol is one of the major products of 1,2-benzenediol
 524 pyrolysis with maximum yield reported at $800\text{ }^\circ\text{C}$ (Ledesma et al. 2002; Thomas et al. 2007). It is
 525 important to note that both temperature and rate of heating influence the composition and yield of
 526 pyrolysis products. Evidenced in Figure 6, the thermal imaging associated with FTIR scan 17

527 shows a temperature of ~200 °C which is indicated in Kibet et al. (2012) to be within the
 528 temperature range of pyrolysis of lignin: 200 to 400 °C. Shortly thereafter, phenol mixing ratios
 529 rapidly increase and reach a maximal mixing ratio of 6.9 ppm at scan 24. At scan 24 the flame
 530 front has already reached the extractive probe and thus the maximum intake of smoke and ambient
 531 air is achieved; temperature of the fuel bed is ca. 600 °C, consistent with the flaming phase. The
 532 gradual decay in phenol production as the flame front passes could be due to several factors: (i) an
 533 increased temperature required for complete combustion of the C₆H₆O (ii) residence time of
 534 phenol, (iii) phenol production in the smoldering phase as a tar/char, (iv) adsorption to walls of the
 535 stainless steel tubing and cell. A cross-section of Figure 6 shows the rapid onset of phenol
 536 production at the temperatures followed by a gradual decay in concentration: this is indicative of
 537 phenol production throughout the burning of inkberry as a species.



538

539 **Figure 7.** Temporal mixing ratios of phenol for different shrub species. Phenol mixing ratios plotted over
 540 time indicated by scan number for Burn 97 sparkleberry (red), Burn 87 inkberry (green), and Burn 20
 541 fetterbush (blue) all on longleaf pine straw bed.

542 The shape of the temporal profile yields information as to the production of phenol throughout the
 543 evolution of burning. Figure 7 shows the progression of phenol concentration following its first
 544 observed presence in the burn. These graphs are effectively a cross-section of Figure 6, showing
 545 the progression of the height of the phenol peak (directly correlated to phenol concentration)
 546 throughout the burn (with time being represented by scan number in both cases). The level of

547 phenol generation was observed to vary between plant species. Temporal profiles of phenol
548 concentration were constructed for burns with three different species: sparkleberry, inkberry, and
549 fetterbush. These plots illustrate a range of behavior with inkberry and sparkleberry having similar
550 temporal profiles and similar maxima of ca. 6.5 ppm and fetterbush having a different temporal
551 profile. It is important to note that Burn 97 was measured at 0.6 cm^{-1} , while burns 87 and 93 were
552 measured at 1.0 cm^{-1} , although the profile of burn 97 is consistent with that of burn 87. [We do not
553 believe the small change in resolution affects the recovered mixing ratios.] Demonstrated in Figure
554 7, trace amounts of phenol appear at the onset of combustion and throughout the pyrolysis phase.
555 Phenol reaches its highest concentrations, however, during the flaming stage as all three temporal
556 profiles reach maximum during the latter stages of the burn. Moreover, phenol remains throughout
557 the duration of the burn and is not consumed by secondary reactions, as is e.g. ethene. For these
558 three burns, fetterbush was observed to have the lowest maximum concentration of phenol, 3.1
559 ppm, of the three species, while sparkleberry and inkberry had similar maxima (as well as similar
560 temporal profiles).

561 The observed differences of phenol in both temporal profile and overall peak concentrations could
562 arise due to differences in leaf structure and shape, or possibly due to differences in leaf/plant
563 composition. Pyrolytic production of phenol has been previously attributed to multiple
564 components of plant composition, including phenol content, lignin content and the amount of
565 cellulose in each plant species. Therefore, varying phenols, lignin, and cellulose in these plant
566 species could be the source of phenol concentration variability for each burn. The physical
567 composition of multiple plant species, including inkberry and fetterbush was analyzed by Matt et
568 al. (2020); it was shown that inkberry has 2.6 times the percentage of phenol by composition
569 (9.0%) than fetterbush (3.4%) Although sparkleberry was not included in that study, it can be
570 suggested that the compositions of inkberry and sparkleberry are similar due to observed phenol
571 in this experiment as well as plant characteristics. Sparkleberry is a member of the *Vaccinium*
572 genus which contains many species collectively known as blueberries which are known to contain
573 high levels of phenolic compounds in the fruits (e.g. Prior et al 1998). This study and the results
574 of Matt et al. support the present hypothesis that peak concentrations of phenol are highest for
575 sparkleberry and inkberry due to higher phenolic content in the plants.

576 **4. Summary**

577 The analytical methods used in this study attempt to provide a detailed view of prescribed burning
578 by enlisting two different FTIR acquisition modes, static and dynamic. By capturing a “snapshot”
579 of a single burn experiment, used in the static method, one can discern the gases with higher
580 specificity and in turn decipher complex spectra by use of chemometrics to extract compounds
581 with high concentrations leaving behind a residual to be analyzed. Lower resolution may hinder
582 these efforts and allow compounds that are present at lower mixing ratios to be obscured by higher
583 absorbing compounds, e.g., carbon dioxide, water, and ethene. In this study we were able to detect
584 additional compounds e.g. phenol, benzene, and allene with greater confidence. However, in
585 gaining specificity there is a loss of time resolution and this is where the dynamic method becomes
586 advantageous. The FTIR dynamic acquisition method when synchronized to thermal imaging,
587 while lower in sensitivity, allows for an overall profile of the burn and can help assign phases to
588 the dynamic stages of the flame. That is, the dynamic method in conjunction with thermal IR
589 imaging provides a more detailed description as temperature and chemical composition profiles
590 can be correlated and assigned to certain phases of the burns. In this study pyrolysis, flaming and
591 smoldering combustion were identified using these new techniques which can aide in the
592 improvement of fire behavior models used by land managers to conduct prescribed fires.

593 *Data availability.* Data are not publicly available as data release has not been authorized by sponsor
594 of this research.

595 *Competing interests.* No competing interests.

596 *Acknowledgements.* This work was supported by the Department of Defense’s Strategic
597 Environmental Research and Development Program (SERDP) within project RC-2640, and we
598 gratefully acknowledge our sponsors for their support. PNNL is operated for the U.S. Department
599 of Energy by the Battelle Memorial Institute under contract DE-AC06076RLO 1830.

600

601 **REFERENCES**

- 602 Agee, J. K.: Fire and pine ecosystems, in *Ecology and Biogeography of Pinus*, edited by D. M.
603 Richardson, pp. 193–218, Cambridge University Press, Cambridge, U.K., 2000.
- 604 Aitchison, J.: *The statistical analysis of compositional data*, Chapman and Hall, London ; New
605 York., 1986.
- 606 Akagi, S. K., Yokelson, R. J., Burling, I. R., Meinardi, S., Simpson, I., Blake, D. R.,
607 McMeeking, G. R., Sullivan, A., Lee, T., Kreidenweis, S., Urbanski, S., Reardon, J., Griffith, D.
608 W. T., Johnson, T. J., and Weise, D. R.: Measurements of reactive trace gases and variable O₃
609 formation rates in some South Carolina biomass burning plumes, *Atmos. Chem. Phys.*, 13, 1141-
610 1165, 2013.
- 611 Akagi, S. K., Burling, I. R., Mendoza, A., Johnson, T. J., Cameron, M., Griffith, D. W. T., Paton-
612 Walsh, C., Weise, D. R., Reardon, J., and Yokelson, R. J.: Field measurements of trace gases
613 emitted by prescribed fires in southeastern US pine forests using an open-path FTIR system,
614 *Atmos. Chem. Phys.*, 14, 199-215, 2014.
- 615 Alves, C. A., Gonçalves, C., Pio, C. A., Mirante, F., Caseiro, A., Tarelho, L., Freitas, M. C., and
616 Viegas, D. X.: Smoke emissions from biomass burning in a Mediterranean shrubland, *Atmos.*
617 *Environ.*, 44, 3024-3033, 2010.
- 618 Aminfar, A., Cobian-Iñiguez, J., Ghasemian, M., Espitia, N. R., Weise, D. R. and Princevac, M.:
619 Using Background-Oriented Schlieren to Visualize Convection in a Propagating Wildland Fire,
620 *Combustion Science and Technology*, 1–21, doi:[10.1080/00102202.2019.1635122](https://doi.org/10.1080/00102202.2019.1635122), 2019.
- 621 Aminfar, A.: *Application of Computer Vision to Transport Phenomena*, Ph.D., University of
622 California, Riverside., 2019.
- 623 Amini, E., Safdari, M.-S., DeYoung, J. T., Weise, D. R. and Fletcher, T. H.: Characterization of
624 pyrolysis products from slow pyrolysis of live and dead vegetation native to the southern United
625 States, *Fuel*, 235, 1475–1491, doi:[10.1016/j.fuel.2018.08.112](https://doi.org/10.1016/j.fuel.2018.08.112), 2019.
- 626 Barbour, M. G. and Billings, W. D., Eds.: *North American terrestrial vegetation*, 2. ed.,
627 Cambridge Univ. Press, Cambridge., 2000.
- 628 Behm, A., Duryea, M. L., Long, A. J. and Zipperer, W. C.: Flammability of native understory
629 species in pine flatwood and hardwood hammock ecosystems and implications for the wildland–
630 urban interface, *International Journal of Wildland Fire*, 13(3), 355–365, doi:[10.1071/WF03075](https://doi.org/10.1071/WF03075),
631 2004.
- 632 Bist, H. D., Brand, J. C. D. and Williams, D. R.: The Vibrational Spectrum and Torsion of
633 Phenol, *J. Mole. Spec.*, 24, 402-412, 1967.
- 634 Biswell, H. H.: *Prescribed burning in California wildlands vegetation management*, Berkeley,
635 CA: University of California Press; p. 255, 1989.

636 Brilli, F., Gioli, B., Ciccioli, P., Zona, D., Loreto, F., Janssens, I. A., and Ceulemans, R.: Proton
637 Transfer Reaction Time-of-Flight Mass Spectrometric (PTR-TOF-MS) determination of volatile
638 organic compounds (VOCs) emitted from a biomass fire developed under stable nocturnal
639 conditions, *Atmos. Environ.*, 97, 54-67, 2014.

640 Burgan, R. E. and Susott, R. A.: Influence of sample processing techniques and seasonal
641 variation on quantities of volatile compounds of gallberry, saw-palmetto and wax myrtle,
642 *International Journal of Wildland Fire*, 1(1), 57–62, doi:[10.1071/WF9910057](https://doi.org/10.1071/WF9910057), 1991.

643 Burling, I. R., Yokelson, R. J., Griffith, D. W. T., Johnson, T. J., Veres, P., Roberts, J. M.,
644 Warneke, C., Urbanski, S. P., Reardon, J., Weise, D. R., Hao, W. M. and de Gouw, J.:
645 Laboratory measurements of trace gas emissions from biomass burning of fuel types from the
646 southeastern and southwestern United States, *Atmos. Chem. Phys.*, 10(22), 11115–11130,
647 doi:[10.5194/acp-10-11115-2010](https://doi.org/10.5194/acp-10-11115-2010), 2010.

648 Burling, I. R., Yokelson, R. J., Akagi, S. K., Urbanski, S. P., Wold, C. E., Griffith, D. W. T.,
649 Johnson, T. J., Reardon, J., and Weise, D. R.: Airborne and ground-based measurements of the
650 trace gases and particles emitted by prescribed fires in the United States, *Atmos. Chem. Phys.*,
651 11, 12197-12216, 2011.

652 Bytnerowicz, A., Arbaugh, M. A., Andersen, C. K. and Riebau, A. R., Eds.: *Wildland fires and
653 air pollution*, Elsevier, Amsterdam ; Boston., 2009.

654 Carter, M. C. and Foster, C. D.: Prescribed burning and productivity in southern pine forests: a
655 review, *Forest Ecol. Manage.*, 191, 93–109, 2004.

656 Christensen, N. L.: Vegetation of the Southeastern Coastal Plain, in *North American Terrestrial
657 Vegetation*, edited by M. G. Barbour and W. D. Billings, pp. 397–448, Cambridge University
658 Press, New York, NY., 2000.

659 Christian, T. J., Kleiss, B., Yokelson, R. J., Holzinger, R., Crutzen, P. J., Hao, W. M., Shirai, T.,
660 and Blake, D. R.: Comprehensive laboratory measurements of biomass-burning emissions: 2.
661 First intercomparison of open-path FTIR, PTR-MS, and GC-MS/FID/ECD, *J. Geophys. Res.*
662 *Atmos.*, 109, 2004.

663 Chi, C. T., Horn, D. A., Zanders, D. L., Opferkuch, R. E., Nyers, J. M., Pierovich, J. M., Lavdas,
664 L. G., McMahon, C. K., Nelson, R. M., Jr., Johansen, R. W. and Ryan, P. W.: Source
665 Assessment: Prescribed Burning, State of the Art, Environmental Protection Technology, United
666 States Environmental Protection Agency, Research Triangle Park, NC. [online] Available from:
667 nepis.epa.gov, 1979.

668 Cohen, S., Hall, J. and Hiers, J. K.: Fire Science Strategy, Strategic Environmental Research and
669 Development Program, Resource Conservation and Climate Change Program Area, Washington,
670 D.C. [online] Available from: [https://serdp-
671 estcp.org/content/download/30210/291748/file/Fire%20Science%20Strategy.pdf](https://serdp-estcp.org/content/download/30210/291748/file/Fire%20Science%20Strategy.pdf), 2014.

672 Collard, F.X. and Blin, J.: A review on pyrolysis of biomass constituents: Mechanisms and
673 composition of the products obtained from the conversion of cellulose, hemicelluloses and
674 lignin. *Renewable and Sustainable Energy Reviews*, 38, pp.594-608, 2014.

675 Crutzen, P. J. and Goldammer, J. G., Eds.: *Fire in the environment: the ecological, atmospheric,
676 and climatic importance of vegetation fires: report of the Dahlem Workshop, held in Berlin, 15-
677 20 March 1992*, Wiley, Chichester, England ; New York., 1993.

678

679 Depew, C. A., Mann, M. J. and Corlett, R. C.: A Laboratory Simulation of Wood Pyrolysis
680 Under Field Conditions, *Combustion Science and Technology*, 6(4), 241–246,
681 doi:[10.1080/00102207208952326](https://doi.org/10.1080/00102207208952326), 1972.

682 Di Blasi, C.: Modeling chemical and physical processes of wood and biomass pyrolysis, *Progress
683 in Energy and Combustion Science*, 34(1), 47–90, doi:[10.1016/j.pecs.2006.12.001](https://doi.org/10.1016/j.pecs.2006.12.001), 2008.

684

685 Dimitrakopoulos, A. P.: Thermogravimetric analysis of Mediterranean plant species, *Journal of
686 Analytical and Applied Pyrolysis*, 60(2), 123–130, doi:[10.1016/S0165-2370\(00\)00164-9](https://doi.org/10.1016/S0165-2370(00)00164-9), 2001.

687

688 Fairburn, J. A., Behie, L. A., and Svrcek, W. Y.: Ultrapyrolysis of n-hexadecane in a novel
689 micro-reactor, *FUEL*, 69, 1537-1545, 1990.

690

691 Frenklach, M., Taki, S., Durgaprasad, M. B., and Matula, R. A.: Soot formation in shock-tube
692 pyrolysis of acetylene, allene, and 1, 3-butadiene, *Combust. Flame*, 54, 81–101, 1983.

693

694 Frenklach, M., Yuan, T., and Ramachandra, M. K.: Soot formation in binary hydrocarbon
695 mixtures, *Energy Fuels*, 2, 462–480, 1988.

696

697 Gilman, J. B., Lerner, B. M., Kuster, W. C., Goldan, P. D., Warneke, C., Veres, P. R., Roberts, J.
698 M., de Gouw, J. A., Burling, I. R., and Yokelson, R. J.: Biomass burning emissions and potential
699 air quality impacts of volatile organic compounds and other trace gases from fuels common in
700 the US, *Atmos. Chem. Phys.*, 15, 13915-13938, 2015.

701

702 Griffith, D. W. T.: MALT5 User guide Version 5.5.9 2016.

703

704 Goode, J. G., Yokelson, R. J., Susott, R. A., and Ward, D. E.: Trace gas emissions from
705 laboratory biomass fires measured by open-path Fourier transform infrared spectroscopy: Fires
706 in grass and surface fuels, *J. Geophys. Res. Atmos.*, 104, 21237-21245, 1999.

707

708 Goode, J. G., Yokelson, R. J., Ward, D. E., Susott, R. A., Babbitt, R. E., Davies, M. A., and Hao,
709 W. M.: Measurements of excess O₃, CO₂, CO, CH₄, C₂H₄, C₂H₂, HCN, NO, NH₃, HCOOH,
710 CH₃COOH, HCHO, and CH₃OH in 1997 Alaskan biomass burning plumes by airborne Fourier
711 transform infrared spectroscopy (AFTIR), *J. Geophys. Res. Atmos.*, 105, 22147-22166, 2000.

712

713 Gordon, I. E., Rothman, L. S., Hill, C., Kochanov, R. V., Tan, Y., Bernath, P. F., Birk, M.,
714 Boudon, V., Campargue, A., Chance, K. V., Drouin, B. J., Flaud, J.-M., Gamache, R. R.,
715 Hodges, J. T., Jacquemart, D., Perevalov, V. I., Perrin, A., Shine, K. P., Smith, M.-A. H.,
716 Tennyson, J., Toon, G. C., Tran, H., Tyuterev, V. G., Barbe, A., Császár, A. G., Devi, V. M.,

717 Furtenbacher, T., Harrison, J. J., Hartmann, J.-M., Jolly, A., Johnson, T. J., Karman, T., Kleiner,
718 I., Kyuberis, A. A., Loos, J., Lyulin, O. M., Massie, S. T., Mikhailenko, S. N., Moazzen-Ahmadi,
719 N., Müller, H. S. P., Naumenko, O. V., Nikitin, A. V., Polyansky, O. L., Rey, M., Rotger, M.,
720 Sharpe, S. W., Sung, K., Starikova, D., S.A. Tashkun, S. A., Van der Auwera, J., Wagner, G.,
721 Wilzewski, J., Wcisło, P., Yu, S., and Zak, E. J.: The HITRAN2016 molecular spectroscopic
722 database, *J. Quant. Spectrosc. Radiat. Transfer*, 203, 3-69, 2017.

723

724 Guérette, É.-A., Paton-Walsh, C., Desservettaz, M., Smith, T. E. L., Volkova, L., Weston, C. J.
725 and Meyer, C. P.: Emissions of trace gases from Australian temperate forest fires: emission
726 factors and dependence on modified combustion efficiency, *Atmos. Chem. Phys.*, 18, 3717-3735,
727 doi: 10.5194/acp-18-3717-2018, 2018.

728

729 Hardy, C. C., Ottmar, R. D., Peterson, J. L., Core, J. E. and Seamon, P.: Smoke management
730 guide for prescribed and wildland fire; 2001 ed., PMS 420-2 National Wildfire Coordinating
731 group, Boise, ID. 226 pp., 2001.

732

733 Hatch, L. E., Yokelson, R. J., Stockwell, C. E., Veres, P. R., Simpson, I. J., Blake, D. R.,
734 Orlando, J. J., and Barsanti, K. C.: Multi-instrument comparison and compilation of non-
735 methane organic gas emissions from biomass burning and implications for smoke-derived
736 secondary organic aerosol precursors, *Atmos. Chem. Phys.*, 17, 1471-1489, 2017.

737

738 Hawthorne, S. B., Krieger, M. S., Miller, D. J., and Mathiason, M. B.: Collection and
739 quantitation of methoxylated phenol tracers for atmospheric pollution from residential wood
740 stoves, *Environ. Sci. Technol.*, 23, 470-475, <https://doi.org/10.1021/es00181a013>, 1989.

741

742 Hough, W. A.: Caloric value of some forest fuels of the southern United States, Research Note,
743 USDA Forest Service, Southeastern Forest Experiment Station, Asheville, NC. [online]
744 Available from: <http://www.treesearch.fs.fed.us/pubs/2778>, 1969.

745

746 Hurst, D. F., Griffith, D. W. T., Carras, J. N., Williams, D. J., and Fraser, P. J.: Measurements of
747 Trace Gases Emitted by Australian Savanna Fires During the 1990 Dry Season, *J. Atmos.*
748 *Chem.*, 18, 33-56, 1994a.

749

750 Hurst, D. F., Griffith, D. W. T., and Cook, G. D.: Trace gas emissions from biomass burning in
751 tropical Australian savannas, *J. Geophys. Res.*, 99, 16441-16456, 1994b.

752

753 Ingemarsson, A., Nilsson, U., Nilsson, M., Pedersen, J. R., and Olsson, J. O.: Slow Pyrolysis of
754 Spruce and Pine Samples Studied with GC/MS and GC/FTIR/FID, *Chemosphere*, 36-14, 2879-
755 2889, 1998.

756

757 Johnson, T. J., Simon, A., Weil, J. M. and Harris, G. W., “Applications of time-resolved step-
758 scan and rapid-scan FT-IR spectroscopy: Dynamics from ten seconds to ten nanoseconds”
759 *Applied Spectroscopy*, 47, 1376, (1993).

760

761 Johnson, T. J., Masiello, T., and Sharpe, S. W.: The quantitative infrared and NIR spectrum of
762 CH₂I₂ vapor: vibrational assignments and potential for atmospheric monitoring, *Atmos. Chem.*
763 *Phys.*, 6, 2581-2591, 2006.

764

765 Johnson, T. J., Profeta, L. T. M., Sams, R. L., Griffith, D.W. T., and Yokelson, R. L.: An
766 infrared spectral database for detection of gases emitted by biomass burning, *Vib. Spectrosc.*, 53,
767 97–102, 2010.

768

769 Jolly, W. M., Hintz, J., Linn, R. L., Kropp, R. C., Conrad, E. T., Parsons, R. A. and Winterkamp,
770 J.: Seasonal variations in red pine (*Pinus resinosa*) and jack pine (*Pinus banksiana*) foliar
771 physio-chemistry and their potential influence on stand-scale wildland fire behavior, *Forest*
772 *Ecology and Management*, 373, 167–178, doi:[10.1016/j.foreco.2016.04.005](https://doi.org/10.1016/j.foreco.2016.04.005), 2016.

773

774 Jolly, W. M., Parsons, R. A., Hadlow, A. M., Cohn, G. M., McAllister, S. S., Popp, J. B.,
775 Hubbard, R. M. and Negron, J. F.: Relationships between moisture, chemistry, and ignition of
776 *Pinus contorta* needles during the early stages of mountain pine beetle attack, *Forest Ecology*
777 *and Management*, 269, 52–59, doi:[10.1016/j.foreco.2011.12.022](https://doi.org/10.1016/j.foreco.2011.12.022), 2012.

778

779 Karl, T. G., Christian, T. J., Yokelson, R. J., Artaxo, P., Hao, W. M., and Guenther, A.: The
780 Tropical Forest and Fire Emissions Experiment: method evaluation of volatile organic compound
781 emissions measured by PTR-MS, FTIR, and GC from tropical biomass burning, *Atmos. Chem.*
782 *Phys.*, 7, 5883-5897, 2007.

783

784 Keresztury, G., Billes, F., Kubinyi, M. and Sundius, T.: A Density Functional, Infrared Linear
785 Dichroism, and Normal Coordinate Study of Phenol and its Deuterated Derivatives: Revised
786 Interpretation of the Vibrational Spectra, *J. Phys. Chem.*, 102, 1371-1380, 1998.

787

788 Kibet, J., Khachatryan, L., and Dellinger, B.: Molecular products and radicals from pyrolysis of
789 lignin, *Environ. Sci. Technol.*, 46, 12994-13001, 2012.

790

791 Kochanov, R.V., Gordon, I.E., Rothman, L.S., Shine, K.P., Sharpe, S.W., Johnson, T.J.,
792 Wallington, T.J., Harrison, J.J., Bernath, P.F., Birk, M. and Wagner, G.: Infrared absorption
793 cross-sections in HITRAN2016 and beyond: Expansion for climate, environment, and
794 atmospheric applications. *Journal of Quantitative Spectroscopy and Radiative Transfer*, 230,
795 pp.172-221. 2019.

796

797 Koss, A. R., Sekimoto, K., Gilman, J. B., Selimovic, V., Coggon, M. M., Zarzana, K. J., Yuan,
798 B., Lerner, B. M., Brown, S. S., Jimenez, J. L., Krechmer, J., Roberts, J. M., Warneke, C.,
799 Yokelson, R. J., and de Gouw, J.: Non-methane organic gas emissions from biomass burning:
800 identification, quantification, and emission factors from PTR-ToF during the FIREX 2016
801 laboratory experiment, *Atmos. Chem. Phys.*, 18, 3299, 2018.

802

803 Ledesma, E. B., Marsh, N. D., Sandrowitz, A. K. and Wornat, M. J.: An experimental study on
804 the thermal decomposition of catechol, *Proceedings of the Combustion Institute*, 29(2), 2299–
805 2306, doi:10.1016/S1540-7489(02)80280-2, 2002.

806

807 Liu, X., Huey, L. G., Yokelson, R. J., Selimovic, V., Simpson, I. J., Müller, M., Jimenez, J. L.,
808 Campuzano-Jost, P., Beyersdorf, A. J., Blake, D. R., Butterfield, Z., Choi, Y., Crouse, J. D.,
809 Day, D. A., Diskin, G. S., Dubey, M. K., Fortner, E., Hanisco, T. F., Hu, W., King, L. E.,
810 Kleinman, L., Meinardi, S., Milkoviny, T., Onasch, T. B., Palm, B. B., Peischl, J., Pollack, I. B.,
811 Ryerson, T. B., Sachse, G. W., Sedlacek, A. J., Shilling, J. E., Springston, S., St. Clair, J. M.,
812 Tanner, D. J., Teng, A. P., Wennberg, P. O., Wisthaler, A., and Wolfe, G. M.: Airborne
813 measurements of western US wildfire emissions: Comparison with prescribed burning and air
814 quality implications, *J. Geophys. Res.-Atmos.*, 122, 6108–6129, doi: 10.1002/2016JD026315,
815 2017.

816
817 Melvin, M. A.: 2015 National Prescribed Fire Use Survey Report, Technical Report, Coalition of
818 Prescribed Fire Councils, Inc. [online] Available from:
819 [http://stateforesters.org/sites/default/files/publication-](http://stateforesters.org/sites/default/files/publication-documents/2015%20Prescribed%20Fire%20Use%20Survey%20Report.pdf)
820 [documents/2015%20Prescribed%20Fire%20Use%20Survey%20Report.pdf](http://stateforesters.org/sites/default/files/publication-documents/2015%20Prescribed%20Fire%20Use%20Survey%20Report.pdf), 2015.

821
822 Matt, F. J., Diitenberger, M. A. and Weise, D. R.: Summative and ultimate analysis of live
823 leaves from southern U.S. forest plants for use in fire modeling, *Energy Fuels*, (34), 4703–4720,
824 doi:[10.1021/acs.energyfuels.9b04107](https://doi.org/10.1021/acs.energyfuels.9b04107), 2020.

825
826 Neuman, J. A., Huey, L. G., Ryerson, T. B., and Fahey, D. W.: Study of Inlet Materials for
827 Sampling Atmospheric Nitric Acid, *Environ. Sci. Technol.*, 33, 1133-1136, doi:
828 10.1021/es980767f, 1999.

829
830 Paton-Walsh, C., Deutscher, N. M., Griffith, D. W. T., Forgan, B. W., Wilson, S. R., Jones, N.
831 B., and Edwards, D. P.: Trace gas emissions from savanna fires in northern Australia, *J.*
832 *Geophys. Res.*, 115, doi:10.1029/2009JD013309, 2010.

833
834 Paton-Walsh, C., Smith, T. E. L., Young, E. L., Griffith, D. W. T. and Guérette, É.-A.: New
835 emission factors for Australian vegetation fires measured using open-path Fourier transform
836 infrared spectroscopy- Part 1: Methods and Australian temperate forest fires, *Atmos. Chem.*
837 *Phys.*, 14, 11313-11333, doi: 10.5194/acp-14-11313-2014, 2014.

838
839 Phillips, M. C., Myers, T. L., Johnson, T. J., and Weise, D. R.: In-situ measurement of pyrolysis
840 and combustion gases from biomass burning using swept wavelength external cavity quantum
841 cascade lasers, *Optics Express*, 28(6), 8680-8700, 2020

842
843 Prior, R. L., Cao, G., Martin, A., Sofic, E., McEwen, J., O'Brien, C., Lischner, N., Ehlenfeldt,
844 M., Kalt, W., Krewer, G. and Mainland, C. M.: Antioxidant Capacity As Influenced by Total
845 Phenolic and Anthocyanin Content, Maturity, and Variety of *Vaccinium* Species, *J. Agric. Food*
846 *Chem.*, 46(7), 2686–2693, doi:10.1021/jf980145d, 1998.

847
848 Pyne, S. J.: *World fire: the culture of fire on earth*, Pbk. ed., University of Washington Press,
Seattle., 1997.

849
850 Rao, P. V. R. and Rao, G. R.: Vibrational analysis of substituted phenols Part I. Vibrational
spectra, normal coordinate analysis and transferability of force constants of some formyl-,

851 methoxy-, formylmethoxy-, methyl- and halogeno-phenols, *Spectrochimica ACTA Part A*, 58,
852 3039-3065, 2002.

853 Roscioli, J. R., Zahniser, M. S., Nelson, D. D., Herndon, S. C., and Kolb, C. E.: New Approaches
854 to Measuring Sticky Molecules: Improvements of Instrumental Response Times Using Active
855 Passivation, *J. Phys. Chem. A*, 120, 1347-1357, doi: 10.1021/acs.jpca.5b04395, 2015.

856 Safdari, M.-S., Rahmati, M., Amini, E., Howarth, J. E., Berryhill, J. P., Diitenberger, M., Weise,
857 D. R., and Fletcher, T. H.: Characterization of pyrolysis products from fast pyrolysis of live and
858 dead vegetation native to the Southern United States, *Fuel*, 229, 151-166, 2018.

859 Safdari, M.-S., Amini, E., Weise, D. R. and Fletcher, T. H.: Comparison of pyrolysis of live
860 wildland fuels heated by radiation vs. convection, *Fuel*, 268, 117342,
861 doi:[10.1016/j.fuel.2020.117342](https://doi.org/10.1016/j.fuel.2020.117342), 2020.

862

863 Saiz-Jimenez, C. and De Leeuw, J. W.: Lignin pyrolysis products: Their structures and their
864 significance as biomarkers, *Organic Geochemistry*, 10(4-6), 869-876, doi:10.1016/S0146-
865 6380(86)80024-9, 1986.

866

867 Scharko, N. K., Oeck, A. M., Myers, T. L., Tonkyn, R. G., Banach, C. A., Baker, S. P., Lincoln,
868 E. N., Chong, J., Corcoran, B. M., Burke, G. M., Ottmar, R. D., Restaino, J. C., Weise, D. R. and
869 Johnson, T. J.: Gas-phase pyrolysis products emitted by prescribed fires in pine forests with a
870 shrub understory in the southeastern United States, *Atmos. Chem. Phys.*, 19(15), 9681-9698,
871 doi:[10.5194/acp-19-9681-2019](https://doi.org/10.5194/acp-19-9681-2019), 2019a.

872 Scharko, N. K., Oeck, A. M., Tonkyn, R. G., Baker, S. P., Lincoln, E. N., Chong, J., Corcoran,
873 B. M., Burke, G. M., Weise, D. R., Myers, T. L., Banach, C. A., Griffith, D. W. T. and Johnson,
874 T. J.: Identification of gas-phase pyrolysis products in a prescribed fire: first detections using
875 infrared spectroscopy for naphthalene, methyl nitrite, allene, acrolein and acetaldehyde,
876 *Atmospheric Measurement Techniques*, 12(1), 763-776, doi:[10.5194/amt-12-763-2019](https://doi.org/10.5194/amt-12-763-2019), 2019b.

877

878 Scott, A. C., Bowman, D. M. J. S., Bond, W. J., Pyne, S. J. and Alexander, M. E.: *Fire on earth:*
879 *an introduction*, John Wiley & Sons, Inc, Chichester, West Sussex., 2014.

880

881 Sekimoto, K., Koss, A. R., Gilman, J. B., Selimovic, V., Coggon, M. M., Zarzana, K. J., Yuan,
882 B., Lerner, B. M., Brown, S. S., Warneke, C., Yokelson, R. J., Roberts, J. M., and de Gouw, J.:
883 High-and low-temperature pyrolysis profiles describe volatile organic compound emissions from
884 western US wildfire fuels, *Atmospheric Chemistry & Physics*, 18, 2018.

885

886 Selimovic, V., Yokelson, R. J., Warneke, C., Roberts, J. M., Gouw, J. d., Reardon, J., and
887 Griffith, D. W. T.: Aerosol optical properties and trace gas emissions by PAX and OP-FTIR for
888 laboratory-simulated western US wildfires during FIREX, *Atmos. Chem. Phys.*, 18, 2929-2948,
889 2018.

890

891 Sharpe, S.W., Sams, R.L., Johnson, T.J., Chu, P.M., Rhoderick, G.C., and Guenther,
892 F.R.: Creation of 0.10-cm⁻¹ resolution quantitative infrared spectral libraries for gas samples,

893 Proc. SPIE 4577, Vibrational Spectroscopy-based Sensor Systems, doi:
894 <https://doi.org/10.1117/12.455730>, 2002.
895
896 Shimanouchi, T.: Tables of Vibrational Frequencies, Consolidated Vol. I. National Bureau of
897 Standards, 1972.
898
899 Smith, T., Paton-Walsh, C. P., Meyer, G. C., Maier, S. W., Russell-Smith, J., Wooster, M., and
900 Yates, C. P.: New emission factors for Australian vegetation fires measured using open-path
901 Fourier transform infrared spectroscopy-Part: Australian tropical savanna fire, *Atmos. Chem.*
902 *Phys.* 14, 14, 11335–11352, 2014.
903
904 Smith, T., Clare Paton-Walsh, C. P. Meyer, Garry Cook, Stefan W. Maier, Jeremy Russell-
905 Smith, Martin Wooster, and Cameron P. Yates. "New emission factors for Australian vegetation
906 fires measured using open-path Fourier transform infrared spectroscopy-Part 2: Australian
907 tropical savanna fires." (2014): 11335.
908
909 Stein, Y. S., Antal Jr, M. J., and Jones Jr., M.: A study of the gas-phase pyrolysis of glycerol, *J.*
910 *Anal. Appl. Pyrol.*, 4, 283–296, 1983.
911
912 Stockwell, C. E., Yokelson, R., Kreidenweis, S. M., Robinson, A. L., DeMott, P. J., Sullivan, R.
913 C., Reardon, J., Ryan, K. C., Griffith, D. W. T., and Stevens, L.: Trace gas emissions from
914 combustion of peat, crop residue, domestic biofuels, grasses, and other fuels: configuration and
915 Fourier transform infrared (FTIR) component of the fourth Fire Lab at Missoula Experiment
916 (FLAME-4), *Atmos. Chem. Phys.*, 14, 9727-9754, 2014.
917
918 Susott, R. A.: Characterization of the thermal properties of forest fuels by combustible gas
919 analysis, *For. Sci.*, 28(2), 404–420, 1982.
920
921 Thomas, S., Ledesma, E. B. and Wornat, M. J.: The effects of oxygen on the yields of the
922 thermal decomposition products of catechol under pyrolysis and fuel-rich oxidation conditions,
923 *Fuel*, 86(16), 2581–2595, doi:10.1016/j.fuel.2007.02.003, 2007.
924
925 Tihay, V. and Gillard, P.: Pyrolysis gases released during the thermal decomposition of three
926 Mediterranean species, *Journal of Analytical and Applied Pyrolysis*, 88(2), 168–174,
927 doi:[10.1016/j.jaap.2010.04.002](https://doi.org/10.1016/j.jaap.2010.04.002), 2010.
928
929 Varhegyi, G., Jakab, E. and Antal, M. J.: Is the Broido-Shafizadeh Model for Cellulose Pyrolysis
930 True?, *Energy Fuels*, 8(6), 1345–1352, doi:[10.1021/ef00048a025](https://doi.org/10.1021/ef00048a025), 1994.
931
932 Viatte, C., Strong, K., Hannigan, J., Nussbaumer, E., Emmons, L. K., Conway, S., Paton-Walsh,
933 C., Hartley, J., Benmergui, J. and Lin, J.: Identifying fire plumes in the Arctic with tropospheric
934 FTIR measurements and transport models, *Atmos. Chem. Phys.*, 15, 2227-2246, doi:, 2015.
935
936 Waldrop, T. A. and Goodrick, S. L.: Introduction to prescribed fires in southern ecosystems,
937 *Science Update*, USDA Forest Service, Southern Research Station, Asheville, NC. [online]
938 Available from: <http://www.treesearch.fs.fed.us/pubs/41316>, 2012.

936 Ward, D. E. and Hao, W. M.: Projections of emissions from burning of biomass for use in
937 studies of global climate and atmospheric chemistry, 19 p., Air and Waste Management
938 Association, Vancouver, British Columbia, Canada. [online] Available from:
939 <http://www.treesearch.fs.fed.us/pubs/43258>, 1991.

940 Ward, D. E., and Hardy, C. C.: Smoke emissions from wildland fires, *Environ. Int.*, 17, 117-134,
941 1991.

942 Ward, D. E. and Radke, L. F.: Emissions measurement from vegetation fires: a comparative
943 evaluation of methods and results, in *Fire in the environment: the ecological, atmospheric, and*
944 *climatic importance of vegetation fires: report of the Dahlem Workshop, held in Berlin, 15-20*
945 *March 1992*, edited by P. J. Crutzen and J. G. Goldammer, pp. 53–76, John Wiley & Sons Ltd.
946 [online] Available from: http://www.fs.fed.us/rm/pubs_other/rmrs_1993_ward_d001.pdf, 1993.

947 Ward, D. E.: Combustion chemistry and smoke, in *Forest Fires: Behavior and Ecological Effects*,
948 edited by E. A. Johnson and K. Miyanishi, pp. 55–77, Academic Press, San Diego, CA. [online]
949 Available from: <http://www.doi.org/10.1016/B978-012386660-8/50006-3>, 2001.

950 Warneke, C., Roberts, J. M., Veres, P., Gilman, J., Kuster, W. C., Burling, I., Yokelson, R., and
951 de Gouw, J. A.: VOC identification and inter-comparison from laboratory biomass burning using
952 PTR-MS and PIT-MS, *Int. J. Mass Spectrom.*, 303, 6–14, doi:10.1016/j.ijms.2010.12.002, 2011.

953 Weise, D. R., Fletcher, T. H., Cole, W., Mahalingam, S., Zhou, X., Sun, L., and Li, J.: Fire
954 behavior in chaparral- Evaluating flame models with laboratory data, *Combust. and Flame*, 191,
955 500-512, <https://doi.org/10.1016/j.combustflame.2018.02.012>, 2018.

956 Weise, D. R., Johnson, T. J. and Reardon, J.: Particulate and trace gas emissions from prescribed
957 burns in southeastern U.S. fuel types: Summary of a 5-year project, *Fire Safety Journal*, 74, 71–
958 81, doi:[10.1016/j.firesaf.2015.02.016](https://doi.org/10.1016/j.firesaf.2015.02.016), 2015.

959 Weise, D. R., Palarea-Albaladejo, J., Johnson, T. J., and Jung, H.: Analyzing Wildland Fire
960 Smoke Emissions Data Using Compositional Data Techniques, *J. Geophys. Res. Atmos.*, 125(6),
961 <https://doi.org/10.1029/2019JD032128>, 2020.

962 Williams, S.D., Johnson, T.J., Sharpe, S.W., Yavelak, V., Oates, R.P. and Brauer, C.S.:
963 Quantitative vapor-phase IR intensities and DFT computations to predict absolute IR spectra
964 based on molecular structure: I. Alkanes. *Journal of Quantitative Spectroscopy and Radiative*
965 *Transfer*, 129, 298-307, <https://doi.org/10.1016/j.jqsrt.2013.07.005>, 2013

966 Yang, H., Yan, R., Chen, H., Lee, D. H. and Zheng, C.: Characteristics of hemicellulose,
967 cellulose and lignin pyrolysis, *Fuel*, 86, 1781–1788, 2007.

968 Yee, L. D., Kautzman, K. E., Loza, C. L., Schilling, K. A., Coggon, M. M., Chhabra, P. S.,
969 Chan, M. N., Chan, A. W. H., Hersey, S. P., Crouse, J. D., Wennberg, P. O., Flagan, R. C., and
970 Seinfeld, J. H.: Secondary organic aerosol formation from biomass burning intermediates: phenol
971 and methoxyphenols, *Atmos. Chem. Phys.*, 13, 8019–8043, [https://doi.org/10.5194/acp-13-8019-](https://doi.org/10.5194/acp-13-8019-2013)
972 2013, 2013.

973 Yokelson, R. J., Griffith, D. W. T. and Ward, D. E.: Open-path Fourier transform infrared studies
974 of large-scale laboratory biomass fires, *Journal of Geophysical Research*, 101(D15), 21067,
975 doi:[10.1029/96JD01800](https://doi.org/10.1029/96JD01800), 1996.

976 Yokelson, R. J., Susott, R., Ward, D. E., Reardon, J., and Griffith, D. W. T.: Emissions from
977 smoldering combustion of biomass measured by open-path Fourier transform infrared
978 spectroscopy, *J. Geophys. Res. Atmos.*, 102, 18865-18877, 1997.

979 Yokelson, R. J., Christian, T. J., Bertschi, I. T., and Hao, W. M.: Evaluation of adsorption effects
980 on measurements of ammonia, acetic acid, and methanol, *J. Geophys. Res.*, 108, 4649,
981 doi:10.1029/2003JD003549, 2003.

982 Yokelson, R. J., Burling, I. R., Gilman, J. B., Warneke, C., Stockwell, C. E., Gouw, J. d., Akagi,
983 S. K., Urbanski, S. P., Veres, P., Roberts, J. M., Kuster, W. C., Reardon, J., Griffith, D. W. T.,
984 Johnson, T. J., Hosseini, S., Miller, J. W., Cocker III, D. R., Jung, H., and Weise, D. R.:
985 Coupling field and laboratory measurements to estimate the emission factors of identified and
986 unidentified trace gases for prescribed fires, *Atmos. Chem. Phys.*, 13, 89-116, 2013.

987 Zhou, X. and Mahalingam, S.: Evaluation of reduced mechanism for modeling combustion of
988 pyrolysis gas in wildland fire, *Combustion Science and Technology*, 171(1), 39–70,
989 doi:[10.1080/00102200108907858](https://doi.org/10.1080/00102200108907858), 2001.

990